

# RADIO INTENSITY AND POLARIZATION DISTRIBUTIONS OF QUASARS AT THREE FREQUENCIES

G.K. MILEY and A.P. HARTSUIJKER  
Sterrewacht, Huygens Laboratorium, Leiden, The Netherlands

Received March 15, 1978

Measurements have been made with the Westerbork Synthesis Radio Telescope of 114 quasars at 4995 MHz, 32 at 1415 MHz, and 22 at 610 MHz. All had known redshifts and 86 were resolved at 4995 MHz. Parameters characterizing the structures are tabulated. For the larger sources ( $>2.5$  beam lengths) the total intensity and where appropriate the polarization distributions are illustrated. A search at 610 MHz for halo emission around eight strong quasars had negative results to a level of about 1 percent.

*Key words:* quasars – radio structures – polarizations

## 1. INTRODUCTION

The decrease of angular size with increasing redshift (e.g. Miley, 1971, Wardle and Miley 1972) is the strongest observed correlation between the radio and optical properties of quasars. Until now angular size was the only parameter of the radio structure to have been studied statistically. With the aim of investigating the statistics of some other parameters which characterise the radio brightness and polarization distributions, we have carried out a series of observations of quasars with the Westerbork Synthesis Radio Telescope (WSRT) at 4995 MHz, 1415 MHz and 610 MHz in all four Stokes parameters.

The observing list was drawn up in 1972 to comprise all radio-strong quasars (flux densities  $\geq 1$  Jy at 178 MHz) whose redshifts were known and whose structure could be resolved by the WSRT. To minimize the necessary observing time any quasar which had previously been shown to emit at least 90% of its 2695 MHz flux from a region smaller than 7 arcsec in size was omitted from the program. The resultant sample then consisted of strong quasars with measured or suspected redshifts and angular sizes which were either larger than 7 arcsec or unknown. This list comprised 114 quasars, all of which were observed at 4995 MHz. Thirty-two of the larger sources were also observed at 1415 MHz and eighteen at 610 MHz. Additional measurements at 610 MHz were carried out on four smaller quasars to search for weak halo radio emission.

The purpose of this paper is to present the results of all these observations. An investigation of possible correlations between the various parameters will be given elsewhere.

## 2. THE OBSERVATIONS

The dates of the observing periods are listed in table 1. As is the usual practise with the WSRT, our 1415 and 610 MHz measurements were interspersed with those from other programs. However, two periods totalling 45 days were dedicated specially to our observations at 4995 MHz.

All of the sources with unknown structure were observed in the first 4995 MHz session for at least three fifteen-minute periods at widely spaced hour angles. For those sources which were found or suspected to be resolved, supplementary observations were carried out in the later session.

In planning the observations we aimed to follow continuously for twelve hours all sources which were both above  $20^\circ$  declination and known to be larger than three beamwidths. For the smaller sources and for sources at lower declinations where the synthesized beam is inevitably complicated, such continuous tracking was not deemed necessary. These resolved small and low declination sources were observed for a total of at least five fifteen-minute periods at widely spaced hour angles in order to obtain two-dimensional coverage of the source structures. Some of the weaker sources were observed for longer periods in order to improve the signal to noise ratio, particularly for the polarization data.

In addition to the regular WSRT calibrators, several additional calibration sources were inserted in order to cover a larger declination range and to monitor the atmospheric effects at 4995 MHz. The observations and data reduction for these calibrators were carried out in as similar a manner as possible to those for the quasars. At all three frequencies 3C 147 was taken as the prime calibrator for flux density and polarization.

### 3. DATA REDUCTION

The WSRT and the associated data reduction package have been described frequently elsewhere (e.g. Baars *et al.* 1973, Högbom and Brouw 1974). Our continuous observations at all three frequencies were reduced using 512 by 512 fast Fourier transforms. The short observations at 610 MHz were processed similarly. However, for the short observations at 4995 and 1415 MHz, economy in the data processing was achieved by operating on smaller fields. Here in most cases 64 by 64 slow Fourier transforms were used, but for a few large sources the field size was increased to 128 by 128. At 610 MHz the density of confusing sources outside the central region of the beam was too large to use the small field transform and even the short observations were handled using 512 by 512 fast transforms.

In all cases the “clean” algorithm (Högbom 1974) was used to remove the effects of sidelobes close to the strong sources and the diffraction grating rings from nearby sources. This algorithm works particularly impressively for the short observations at 610 MHz. Figure 1 shows an example of the effect of cleaning for the sources 1425+26.

The measured flux densities and polarizations for the secondary calibrators are given in table 2. The positions were calibrated with reference to calibrator positions measured with the Cambridge 5 km Telescope (Ryle and Elsmore 1973) or the NRAO interferometer (Wade 1970). For the larger sources ( $> 1.5$  beamwidths) the morphological parameters were derived from the maps, while for the slightly resolved sources these parameters were estimated by modelling the visibility data.

### 4. RESULTS

#### a) Tables

Measured parameters for all the sources are given in table 3. For each source we list the integrated source parameters on the first two lines and for those sources that are sufficiently resolved we list the parameters pertaining to the west (W) central (C) and east (E) components below. Doubtful quantities are enclosed by parentheses. The columns of table 3 are as follows:

1. The source name in the notation of the Parkes Catalogue.
2. Indication as to whether the source is included in the 3C, 4C, Parkes (PKS) and Bologna (B) catalogues. Other source names can be found in Burbidge *et al.* (1977).
- 3–8. Above. The position of the optical QSO referred to epoch 1950.0.  
This is accurate to better than half an arcsec.  
Below. The displacement of the outer component edges in arcsec with respect to the optical position. Uncertainties are typically 0.5'' in right ascension and 0.5'' cosec  $\delta$  in declination  $\delta$ .
- 9–16. The 4995 MHz data.
  9. Above. The number of times the source was observed multiplied by the average numbers of minutes per observation.  
Below. The shortest spacing in meters at which data was obtained.
  10. The peak brightness in mJy per beam area.
  11. Above. The coherently averaged fringe amplitude observed at the shortest spacing. At 4995 MHz (where in general there is no significant confusion from background sources in the field), this will be approximately equal to the integrated flux density except for the largest sources. For a source of 10 beam extensions the short spacing (36 m) fringe amplitude will be smaller by  $\sim 10\%$ .

Below. The flux density of the individual components in mJy.

These were calculated by summing the intensity matrix contained by each component and normalizing by the sum of the intensities in the restoring beam.

- 12–13. The polarization percentage and position angle in degrees.
14. The observed angular extent of the whole source (above) and the individual components (below) in arc secs. For some low declination sources we effectively measure the angular extent only in the east-west (EW) direction, since the beam size is a factor  $\text{cosec } \delta$  larger in declination  $\delta$  than in right ascension. Where appropriate this EW angular extent is given. Also note that the estimate of angular extent is inevitably influenced by the sensitivity and dynamic range of the instrument. Since the quasars are almost all luminous radio sources in which the relatively bright outer regions of emission dominate, the overall angular extent is not very sensitive to this selection effect. However our estimate of component size is very dependent on the relative importance of a radio ridge (see below) and is therefore highly subjective. The values of component extent should be treated with the greatest of caution.
15. Above. The number of half power beamlengths covered by the source, measured along the source axis. At 4995 MHz the half power beam is an ellipse  $6''$  in right ascension by  $6'' \text{ cosec } \delta$  in declination. Below. For sources larger than 7 beam lengths a qualitative distinction is made between those having pronounced bridges connecting their outer edges to the central components (denoted by 'b') and those without pronounced bridges (denoted by 'c').
16. The position angle of the source extension in degrees.
- 17–20. The 1415 MHz data, where measured.
- 21–24. The 610 MHz data, where measured.
25. The redshift (Burbidge *et al.* 1977; Hawley, *et al.* 1977; Wills and Lynds 1978). In the case of 1415 and 610 MHz data there is sometimes a discrepancy between the values in column 18 and 22 for the integrated source flux density derived by summing the flux densities of the individual components (below) and their short spacing fringe amplitudes (above). This is due to the presence of confusing sources in the field of the primary beam (whose area is larger by a factor 67 at 610 MHz than at 4995 MHz).

The uncertainties listed in table 3 include the effects of noise and calibration. It is difficult to quantify the errors introduced into the parameters by the somewhat subjective division of the source into components or by the clean procedure. Therefore, both these effects have not been included in the uncertainty estimates.

## b) Diagrams

The intensity distributions of all sources larger than 2.5 beam lengths are shown as contour maps in figure 2. Because so many of the sources are at low declination the declination scale has been compressed by  $\text{cosec } \delta$  to give a circular beam appearance. The primary contour interval in mJy per beam area is indicated on the top right corner of each contour diagram and possible additional contour levels are shown at the top left corner. Where there is significant polarization distribution information, this is given next to the total intensity distribution. The vector polarizations are marked on contour diagrams of polarized intensity; the contour levels being indicated in the same way as for the total intensity maps. Here also compressed declination scales are used but the angles of the vectors are uncompressed values, i.e. they are the polarization angles measured on the sky.

## 5. COMMENTS ON INDIVIDUAL SOURCES

- 0003+15 Possibly faint extensions to southeast extending  $\sim 45''$  from qso containing  $\sim 20$  mJy at 5 GHz ( $\sim 5\%$  of total source flux). The west component was below the brightness limit of Macdonald and Miley (1971) who therefore underestimated the overall source size.

- 0133+20 Note the twofold rotational symmetry (S-shape). Both components are elongated in same direction differing from the overall source orientation. Also, the polarization vectors indicate that the magnetic field direction traces around the edge of the eastern component.
- 0135-057 This QSO (PHL 1078) was thought to be associated with 4C-05.06 (e.g. Burbidge 1977). However, at 5 GHz no radio emission  $>10$  mJy per beam was found within  $1'.5$  of optical position.
- 0137+012 The existence of the west component is uncertain.
- 0214+10 Because of solar interference, the 1.4 GHz map was made without data from shorter baselines. The "hot spot" in the easterly component is less prominent than that in the westerly one. Because of this the easterly component fell below the brightness limit of Macdonald and Miley (1971) who therefore underestimated the overall source size.
- 0232-02 There is possibly an additional component  $\sim 28''$  to west containing  $\sim 20$  mJy at 5 GHz ( $\sim 7\%$  of total source flux).
- 0350-07 The westerly component was below the brightness limit of Macdonald and Miley (1971) who therefore underestimated the overall size.
- 0812+02 An additional component  $550''$  away was noted by Macdonald and Miley (1971). This component was detected to the east of the qso (pa  $80^\circ$ ), was unresolved with a flux density of  $\sim 800$  mJy at 0.6 GHz and is presumably an unrelated background source.
- 0833+65 Note that peak of west component is  $\sim 13''$  from the qso and not at outer edge of radio source.
- 0846+10 There is possibly a weak extension to  $\sim +90''$  in an easterly direction containing  $\sim 40$  mJy at 1.4 GHz.
- 0850+14 There is possibly a weak extension of west component to  $-7''$  containing  $\sim 15$  mJy at 5 GHz ( $\sim 9\%$  of total source flux).
- 0903+16 There is possibly a weak extension to  $\sim -45''$  west of qso containing  $\sim 25$  mJy at 5 GHz ( $\sim 5\%$  of total flux).
- 1004+13 Note the twofold rotational symmetry as for 0133+20.
- 1012+48 Note that for the 5 GHz data, the 36 m fringe amplitude exceeds the sum of the component flux densities. The difference may be in a smooth bridge which is resolved out by the WSRT.
- 1047+09 The 1.4 GHz data is based on a single 15 min observation. The other 1.4 GHz observations of this source were damaged by solar interference.
- There are several ways in which the morphology of this source can be interpreted.
- Component 'C' includes the eastern component associated with the qso and component 'W' is an unrelated source. Since there is evidence for a bridge joining C and W we do not consider this possibility to be very likely.
  - Component 'C' includes the eastern component of the source. The spatial asymmetry would then exceed a factor of 20.
  - The eastern component (if any) is below the detection limit implying a W to E flux ratio  $>6$  at 5 GHz. We have adopted this third alternative as the likeliest.
- The morphology of this source is further complicated by an additional point component containing  $95 \pm 10$  mJy detected on the 0.6 GHz map to the west of the qso ( $\sim 8'$  in pa  $125 \pm 3^\circ$ ). The pa agrees well with that of the source listed in table 2. However, on statistical grounds this component is probably an unrelated source.
- 1100+77 About 92% of the 5 GHz source flux is contained in the  $21''$  structure. However definite weak emission extends outwards from both the west and east hot spots. Taking this into account the overall size of the source (bracketted value) is  $48''$ . The larger extent is evident on both the 5 and 1.4 GHz data. Here is a good example of the dependence on source size on instrumental sensitivity.

- 1217+02 At 5 GHz the difference between the 72 m fringe amplitude (upper value) and the map flux density (lower value) indicates that this source may be slightly resolved. On a larger scale the 1.4 and 0.6 GHz data both suggest extensions  $\sim 50''$  to both east and west containing an extra flux density of  $\sim 50$  and  $\sim 150$  mJy respectively at 1.4 and 0.6 GHz. Due to the low declination this could be a residual of the cleaning procedure. However, we note that Macdonald and Miley (1971) also claimed this source to be extended by  $\sim 150''$  at 2.7 GHz.
- 1232-24 The 1.4 GHz data indicate that the southeastern component possibly extends by an additional  $\sim 1.5'$ .
- 1327-21 The brightness distribution probably tails off gradually into the noise. The southeastern component may have an additional weak extension further to the south.
- 1425+26 The eastern component is resolved out below the detection limit of the full resolution 5 GHz map. This component is visible on the convolved 5 GHz and the full resolution 1.4 and 0.5 GHz maps. The 5 GHz parameters for this source have therefore been taken from the convolved map. Note that the core extension visible on the 1.4 GHz map coincides well in position angle with the elongation of the westerly component from the high resolution 5 GHz map. This may indicate that the qso has undergone significant translational motion in this direction during the lifetime of the radio source.
- 1449-012 At 5 GHz the difference between the 72 m fringe amplitude (upper value) and the map flux density (lower value) indicates that the source may be slightly resolved.
- 1451+09 Apparent extension of the core may be due to the addition of the central part of the bridge to the core component.
- 1512+37 Note the two-dimensional rotational symmetry.
- 1634+26 Note the clumpy bridge. The clumps were included in the individual components when making the estimates of component size. Note also the symmetry apparent in the west and east clumps. The westerly component was below the brightness limit of Macdonald and Miley (1971) who therefore underestimated the overall size.
- 1704+60 The northeastern component has a complex structure in both total intensity and polarization. The component size listed refers to the hot spot.
- 2135-14 Note the symmetry between the clumps in the western and eastern components.
- 2225-05 There is a 40 mJy source  $196''$  west of given position. This is presumably the 4C source. Otherwise no emission  $> 15$  mJy per beam was detected within  $4'$  of the qso.
- 2251+11 Macdonald and Miley (1971) listed this source as having an angular size of  $\sim 8''$ . This probably indicates the presence of a strong central component and that the western component was below the brightness limit of Macdonald and Miley.
- 2308+09 This is one of the few sources in which the western component is at a different angle with respect to the core than the eastern component.
- 2321-24 At 5 GHz this may be slightly resolved. Because of the low declination we give only an upper limit to the size.

## 6. GENERAL COMMENTS ON THE MORPHOLOGIES

The statistics of the various morphological parameters will be dealt with elsewhere. Here we make a few general comments about the morphologies.

(i) Almost always the brightest radio regions occur close to the outer edges of the sources. This is to be expected from the correlation between radio luminosity and morphology first noted by Fanaroff and Riley (1974). Prominent exceptions are 1100+77 and 1327-21.

(ii) Two-dimensional rotational symmetry is exhibited by 0133+20, 1004+13 and 1512+37. In each case both components are aligned in the same direction which differs from that of the overall source orientation.



This symmetry (e.g. Miley 1976) may indicate that here the axis of the radio production mechanism may have changed in direction within the lifetime of the source.

(iii) The agreement in orientation of the core and hot spots of 1425+26 indicates that the qso may have undergone significant translational motions during the lifetime of the source.

(iv) The symmetry between the west and east clumps of 1634+26 and 2135-14 suggests that such clumps are remnants of enhanced activity within the central qso rather than produced by an effect of the external environment.

(v) Central radio components were detected in 38 of the 43 sources that were sufficiently resolved at 4995 MHz. The only quasars with central components weaker than 3% of the total source intensity are 0710+11, 1012+48 and 1704+60. The rate of detection of these radio cores is strikingly higher than for radio galaxies (e.g. Fanti and Perola 1977), suggesting a definite correlation between the intensities of compact optical and compact radio emissions.

(vi) The polarization data indicate that the magnetic field directions are aligned along the radio bridges and curve around at the hot spots, tracing out the total intensity distributions of the sources. Similar behaviour has also been noted by Miley (1976) and Willis and Strom (1977).

## 7. A SEARCH FOR HALO EMISSION

It is now generally believed that the radio source mechanism is a quasi-continuous process. Energy is channelled outwards from the nuclear machine to the regions of bright emission found at the outer edges of the more luminous sources. The spectral data indicate that the ages of the radiating electrons in the hot spots are much shorter than the total lifetime of the radio source. One can then ask whether remnants of a post radio phase might be located in the form of a weak radio halo beyond the hot spots which at present dominate the source morphology. An example of where such structure can be seen is in 1100+77 (figure 2). Such remnant halos would be comprised of old electrons and would have relatively steep non-thermal spectra.

Another case where one might fruitfully search for weak halo emission is close to compact sources with flat radio spectra. Just as extended sources have in recent years been unexpectedly found to have flat spectra compact components embedded within them, so also the compact sources might have weak extended emission associated with them which could be masked by the relatively strong compact cores.

Because of the normally good gain and phase stability of the associated electronics and due to the usually stable Dutch weather conditions, the WSRT is an excellent instrument for searching for weak emission close to strong radio sources. For the above reasons eight quasars of varying morphological types were observed for 12 hour periods with the WSRT at 610 MHz. The results are shown in table 4. Although we reached a level in rightness per beam of about 1 percent of the total source flux density, no extended halo emission was found. In a few cases  $\sim 100$  mJy sources were found within a few arcmin of the quasar. However, the density of these "companion" sources was no greater than the chance coincidence rate to be expected from source count statistics, in agreement with the result of Van Vliet *et al.* (1976) obtained from a study of strong sources observed with the WSRT at 1415 MHz. We found no ridges connecting these "companion" sources to the qso nor did we notice any peculiar configurations. Within about two beamwidths of the known strong radio sources (near field) we can place an upper limit to the brightness level of an extended halo of about 1.5% of the total source flux density. Outside this region (far field) our limits are typically a factor of three better. The last column of table 4 gives in parentheses the distance from the quasar to the closest observed "companion" source.

## ACKNOWLEDGEMENTS

We are grateful to all our colleagues at Westerbork Dwingeloo and Leiden who made these observations possible and particularly acknowledge the help of Dr. P. Katgert and several useful discussions with

Professor H. van der Laan, J. Wouterlood and Miss P. van Yperen assisted with the reduction and the figures were produced with the patient and painstaking assistance of J. Ober and L. Zijderduin. The manuscript was partially typed at Lick Observatory while one of us (GKM) was there on sabbatical leave. The Westerbork Synthesis Radio Telescope is operated by the Netherlands Foundation for Radio Astronomy with financial support from the Netherlands Organization for the Advancement of Pure Research (Z.W.O.).

## REFERENCES

- Baars, J.W.M., van der Brugge, J.F., Casse, J.L., Hamaker, J.P., Sondaar, L.H., Viseer, J.J. and Wellington, K.J.: 1973, *Proc. Inst. Elec. Electron. Engr.* **61**, 1258.
- Burbidge, G.K., Crowne, A.H. and Smith, H.E.: 1977, *Astrophys. J. Suppl.* **33**, 113.
- Fanaroff, B.L. and Riley, J.M.: 1974, *Monthly Notices Roy. Astron. Soc.* **167**, 31P.
- Fanti, R. and Perola, G.C.: 1977, in D. Jauncey (ed.), *Proc. I.A.U. Symp.*, 74 Reidel.
- Hawley, S.A., Miller, J.S. and Weymann, R.J.: 1977, *Astrophys. J.* **213**, 632.
- Högbom, J.A. and Brouw, W.: 1974, *Astron. Astrophys. Suppl.* **15**, 417.
- Högbom, J.A.: 1974, *Astron. Astrophys.* **33**, 289.
- Macdonald, G.H. and Miley, G.K.: 1971, *Astrophys. J.* **164**, 237.
- Miley, G.K.: 1971, *Monthly Notices Roy. Astron. Soc.* **164**, 237.
- Miley, G.K.: 1976, in G. Setti (ed.), *Proc. Physics of non-thermal radio Sources*, Reidel.
- Ryle, M. and Elsmore B.: 1973, *Monthly Notices Roy. Astron. Soc.* **164**, 223.
- Shaffer, B.B., Kellermann, K.I., Purcell, G.H., Paulin-Toth, I.I.K., Preuss, E., Witzel, A., Graham, D., Shilizzi, R.T., Cohen, M.H., Moffet, A.T., Romney, J.D. and Neill, A.E.: 1977, *Astrophys. J.*, in press.
- Wade, C.M.: 1970, *Astrophys. J.* **162**, 381.
- Wills, D. and Lynds, R.: 1977, *Astrophys. J.*, in press.

G.K. Miley

Lick Observatory  
University of California  
Santa Cruz, Ca. 65064 (USA)

A.P. Hartsuijker

Sterrewacht  
Huygens Laboratorium  
Leiden (The Netherlands)

Table 1 Dates of the observations

4995 MHz <sup>a</sup>	1415 MHz	610 MHz
29 March-21 April 1973	13 April-3 November 1971	3 June-12 June 1974
12 April-3 May 1974	3 July-27 October 1974	25 January-10 June 1975

<sup>a</sup> Periods dedicated to this project.

Table 2 Flux densities and linear polarizations of the calibrators<sup>a</sup>

Source	4995 MHz <sup>b</sup>			1415 MHz <sup>d</sup>			610 MHz <sup>d</sup>		
	Flux Density (Jy)	Polarization		Flux Density	Polarization		Flux Density	Polarization	
		perc.	p.a.(deg)	(Jy)	perc.	p.a.(deg)	(Jy)	perc.	p.a.(deg)
0134+32 (3C48)	5.59±0.17	4.9±0.4	106±5	(15.67)	(0.0)		29.0±1.0	0.1±0.5	48±290
PKS 0237-23	3.02±0.09	5.3±0.4	146±4						
0316+16 (CTA 21)	3.00±0.09	0.6±0.4	91±40						
0538+49 (3C147)	(8.18)	(0.0)		(21.57)	(0.0)		(37.78)	(0.0)	
PKS 1148-00	1.89±0.06	4.5±0.4	149±5						
1328+30 (3C286)	7.81±0.23	10.5±0.4	33±2						
1458+71 (3C309.1)	3.73±0.11	2.0±0.4	54±11						
1730-13 (NRAO 530) <sup>c</sup>	4.85±0.30	3.6±0.5	68±8						
2251+15 (3C454.3)	11.6±0.35	3.3±0.4	9±7						

<sup>a</sup> Referenced to 3C147 at 4995 MHz and 610 MHz and 3C48 and 3C147 at 1415 MHz.  
<sup>b</sup> Mean of two observing sessions.  
<sup>c</sup> The flux density of NRAO 530 differed significantly between the two 4995 MHz sessions.  
<sup>d</sup> Regular WSRT calibrators.

Table 4 Limits to halo emission at 610 MHz.

Source	Alt names	Flux Density (mJy)	Size (arcsec)	Region (arcsec)	Near Field	
					Brightness limit (mJy/beam)	Far Field Brightness limit (mJy/beam)
0017+15	4C 15.01, PKS	5090	8.3	90x180	< 60	< 35 (15')
0802+10	3C 191, 4C 10.25, PKS	4315	1.2	90x270	< 60	< 30 (12')
0937+39 <sup>a</sup>	4C 39.27	986	50	100x125	< 30	< 12 (5')
1012+48	4C 48.28	1327±70	109	90x130	< 35	< 10 (6')
1328+30	3C 286, 4C 30.26	28060	0.07	90x180	< 250	< 90 (8')
1512+37	4C 37.43	1725±100	55	100x120	< 30	< 10 (6')
1545+21	3C 323.1, 4C 21.45, PKS	4667±250	69	90x250	< 60	< 40 (20')
1641+39 <sup>b</sup>	3C 345, 4C 39.48	7105±350	0.001	See note		< 35 (5')

<sup>a</sup> 0937+39 Three weak sources (<100 mJy) are found between 5' and 10' from the qso. The position angle of the qso does not align with the position of these sources and no connecting bridge was seen.

<sup>b</sup> 1641+39 May be slightly resolved in the north-south direction (~200 mJy in 30").

A 50 mJy point source is found 4.5' from the qso in p.a.  $147^\circ \pm 6^\circ$ .

This should be compared with a position angle of  $106^\circ$  for the central component of 3C 345 (Shaffer *et al.*, 1977). No connecting bridge was seen.



Table 3

Source	Alt. Names	Position (1950)			Decr. d m s	Obs. Time (Min. Basel)	4995 MHz Flux Density (mJy)		Polarization		Extension			1415 MHz Flux Density (mJy)		Polarization		Obs. Time (min.) (72 m)	610 MHz Flux Density (mJy)		Redshift
		R.A. h m s	b m s	l m s			Peak	Total	perc.	P.A. (deg)	arc sec	arc min	arc sec	P.A. (deg)	perc.	P.A. (deg)	Obs. Time (min.) (72 m)		Obs. Time (min.) (72 m)	perc.	
2003+15	4C 15-01 PKS	00 03 25.01	+15 53 06.6	+210	5x24 (72 m)	48	76±10	<11	31.5±1.8	4.8	11.5±6									0.450	
0017+15	3C 9 4C 15-02 PKS	00 17 49.94	+15 24 16.2	-710	6x30 (72 m)	105	169±20	<5	8.3±2	1.0	137±15									2.017	
0110+29	4C 29-02 PKS	01 10 38.61	+29 26.0	-210	6x15 (72 m)	55	68±5	<15	76.2±1.6	9.6	41.6±1.2									0.763	
0113+02	3C 37 4C 02-04 PKS	01 13 43.63	+02 42 19.9	+315	6x32 (72 m)	160	182±10	8.6±1.9	15.4±2.2	2.8±8	166±20									0.612	
0118+03	3C 39 4C 01-02 PKS	01 18 26.05	+03 28 32.2	+810	6x32 (72 m)	300	325±16	<3	15.3±1.0	7.1	105±21									0.765	
0130+24	4C 24-02 PKS	01 30 39.05	+24 12 19.0	-115	6x15 (72 m)	55	23±13	<18	34.6±1.0	9.1	93±5									0.437	
0133+20	3C 47 4C 20-07 PKS	01 33 40.43	+20 42 10.30	-915	1x720 (72 m)	425	712±33	7.2±0.5	3.5±0.7	33±9	68±2	7.3	35.0±1.5	1x720 (198 m)	3609±181	4.6±0.7	177±9	6x15 (72 m)	8800±440	<1.5	0.425
0141+33	4C 31-03 B2	01 41 06.55	+33 56 54.2	+110	3x15 (72 m)	410	462±24	<3												1.455	
0202+17	PKS	02 02 36.55	-17 13 39.1	+235	3x15 (72 m)	300	302±20	10.7±1.4	1.8±4.8											1.740	
0214+10	4C 10-06 PKS	02 14 26.6	+10 50 18.3	-605	3x15 (72 m)	1300	1300±70	5.2±0.5	1.0±5											0.408	
0223+01	4C 01-11 PKSM	02 23 35.03	-01 24 03.9	+225	6x15 (72 m)	110	204±11	<5	11.9±2	19.2	75±3									2.037	
0232+04	4C 32-06 PKS	02 32 36.51	-04 15 10.12	-575	3x15 (72 m)	125	130±12	<8	14.5±4.2	1.8	47±9									1.636	
0232+07	4C 02-12 PKSM	02 33 00.56	-02 32 34.8	-1010	6x15 (72 m)	195	200±11	<6	1.0±3.6	0.8										1.322	
0235+00	PKSM	02 35 55.09	-00 31 53.9	+210	3x15 (72 m)	183	220±12	<10												1.998	
0317+02	4C 17-02 PKSM	03 17 58.06	-02 19 25.1	-210	6x15 (72 m)	230	260±14	<5												2.092	
0334+12	B2	03 33 22.47	+12 08 36.7	+210	7x45 (72 m)	2310	2600±130	4.8±0.5	5.9±6											1.258	
0349+14	3C 95 PKS	03 49 09.45	-14 38 06.4	-3010	6x15 (72 m)	135	590±30	<8	11.4±4	6.8	165.5±0.7									0.614	
0350+07	3C 94 PKS	03 50 03.97	-07 19 57.4	-585	6x15 (72 m)	187	372±19	5.7±0.9	1.70±9											0.962	
0405+12	PKS	04 05 27.46	-12 19 32.3	+210	6x15 (72 m)	465	562±28	11.3±0.7	9.5±4											0.574	
0454+039	PKSM	04 54 08.33	+35 15.7	-1110	6x15 (72 m)	405	450±24	5.3±1.2	8.2±13											1.345	
0624+44	08 471	06 42 13.1	+44 54 30.0	-310	6x15 (72 m)	840	910±46	1.6±0.5	139±18											3.402	
0704+28	B2	07 04 08.4	+28 26 57.3	+210	6x15 (72 m)	114	128±8	<12	20.6±1.0	3.4	83±4									0.579	

Table 3 (continued)

Source	Alt. Names	Position (1950)			R.A. h m s	Dec. d m s	Obs. Time (Min-Basel)	Flux Density (mJy)		Polarization		Extension		Obs. Time (Min-Basel)	1.15 MHz Flux Density (mJy)		610 MHz Flux Density (mJy)		Redshift
		u	v	total				perc.	p.a. (deg)	arc sec	arc beam	p.a. (deg)	Obs. Time (Min-Basel)		perc.	p.a. (deg)	Obs. Time (Min-Basel)	perc.	
0710+11	3C 175 4C 11.26 PKS	07 10 15.33	+11 51 22.9	-22°55'	-11°10'	7x15 (72 m)	630±22	<10	47±2	6.6	59±5	5x15 (72 m)	2316±15	< 2.7	0.768				
0711+35	01 318	07 11 05.61	+35 52.6	+18°00'	+18°00'	3x15 (72 m)	300±16	7.1±1.5	5±3	130±10	5x15 (72 m)	960±18	2.2±0.7	8±18					
0718+31	07 38	07 18 00.74	+31 19.0	+0°00'	+0°00'	3x15 (72 m)	158±6	16.7±1.2	7±3	90±10	5x15 (72 m)	1440±72	< 1.8	1.620					
0803+04	4C 05.34	08 05 19.17	+04 20.5	+0°00'	+0°00'	6x15 (72 m)	2170	2265±113	4±6	u	u	1800±200	2.7±0.5	3x10					
0812+02	4C 02.73 PKS PKS PKS	08 12 47.28	+02 04 11.7	+1°15'	+1°15'	6x15 (72 m)	652	850±42	2±10	0.8	170±40	1x720	2402±120	3.1±0.8	11±15				
0814+22	3C 197 4C 22.20	08 14 38.15	+22 46 38.6	+1°10'	+1°10'	6x15 (72 m)	500±100	< 3	23±3	1.5	171±3	1800±200	2.7±0.5	3x10					
0833+65	3C 204 4C 65.09	08 33 18.03	+65 24 04.4	+1°15'	+1°15'	1x720 (72 m)	302	304±16	3±4	6.0	94±2	5x15 (72 m)	1100±55	< 5	1.112				
0835+58	3C 205 4C 58.16	08 35 09.94	+58 04 51.8	+1°10'	+1°10'	6x15 (72 m)	130	188±10	6±2	90±10	6±2	670±33	< 3	1.534					
0836+19	4C 19.31	08 36 15.00	+19 32 24.4	+3°10'	+3°10'	6x15 (72 m)	380	416±22	1±4	2.3	134±4	1±4	482±24	< 3	2.691				
0837+12	3C 206 PKS	08 37 27.96	-12 03 53.9	+3°10'	+3°10'	6x15 (72 m)	<10	80±5	16±1	80±5	16±1	80±5	16±1	80±5					
0846+10	4C 09.31 PKS	08 46 57.61	+10 00 32.3	+0°00'	+0°00'	1x720 (72 m)	27	98±50	3±4	28.2	90±2	1x720	131±65	3.2±0.8	108±14				
0850+12	3C 208 4C 14.28 PKS	08 50 22.63	+12 04 16.5	+0°00'	+0°00'	6x30 (72 m)	135	126±8	11±1	1.2	33±10	4x15	53±26	< 12	0.366				
0856+17	4C 17.46	08 56 04.29	+17 03 07.6	+4°05'	+4°05'	6x15 (72 m)	117	172±9	1±5	1.2	33±10	4x15	53±26	< 12	0.366				
0903+16	3C 215 4C 16.26 PKS	09 03 44.23	+16 38 16.4	+1°10'	+1°10'	6x30 (72 m)	30	557±30	7±6	3.7	138±4	3x23	451±25	< 30	0.411				
0906+01	4C 01.24 PKS PKS	09 06 35.16	+01 33 48.0	+0°00'	+0°00'	6x15 (72 m)	115	214±11	1±1	4.3	143±10	6±3	143±10	< 5	1.018				
0911+05	4C 05.38	09 11 24.0	+05 20 17.0	+0°05'	+0°05'	6x15 (72 m)	800	883±45	5±2	2.8	20±2	4x15	53±26	< 12	0.303				
0922+14	4C 14.31 PKS	09 22 22.41	+14 57 23.2	+0°05'	+0°05'	1x720 (72 m)	179	205±11	1±5	1.5	04±0	9±20	1.5	04±0					
0927+36	3C 208.2 4C 36.15	09 27 23.95	+36 14 36.7	+0°00'	+0°00'	6x15 (72 m)	62	69±6	4±8	2.8	20±2	40±4	2.8	20±2					
0928+02	4C 02.27 PKS PKS	09 28 42.93	+02 17 38.6	+0°00'	+0°00'	7x15 (72 m)	105	147±8	6±2	5.2	56±31	5x15	728±37	5.4±2.6	140±28				
0933+39	4C 39.27	09 33 58.20	+39 07 30.0	+0°00'	+0°00'	1x720 (72 m)	47	70±5	7±12	4.3	100±20	5x15	728±37	5.4±2.6	140±28				
0933+25	0K 290	09 33 58.20	+39 07 30.0	+0°00'	+0°00'	6x15 (72 m)	105	147±8	6±2	5.2	56±31	5x15	728±37	5.4±2.6	140±28				
0937+00	4C 00.34 PKS	09 37 43.75	+00 19 43.2	+0°00'	+0°00'	6x15 (72 m)	32	37±3	3±2	1.3	100±20	5x15	728±37	5.4±2.6	140±28				
0937+09	4C 09.35	09 37 43.75	+09 19 43.2	+0°00'	+0°00'	6x15 (72 m)	49	122±4	4±6	1.3	100±20	5x15	728±37	5.4±2.6	140±28				
0937+25	0K 290	09 37 43.75	+25 19 43.2	+0°00'	+0°00'	6x15 (72 m)	103	164±8	4±6	5.0	44±9	6x15	728±37	5.4±2.6	140±28				
0937+00	4C 00.34 PKS	09 37 43.75	+00 19 43.2	+0°00'	+0°00'	6x15 (72 m)	78	108±6	4±6	5.0	44±9	6x15	728±37	5.4±2.6	140±28				

Table 3 (continued)

Source	Alt. Names	Position (1950)			DEC.		Obs. Time (Min. Base)	4985 MHz Flux Density (mJy)		Polarization		Extension			1415 MHz Flux Density (mJy)		Polarization		610 MHz Flux Density (mJy)		Redshift					
		R.A. h m s	d	m s	h	m s		Peak	Total	perc.	p.a. (deg)	arc sec	arc min	arc sec	perc.	p.a. (deg)	Obs. Time (min.)	Flux Density (mJy)	perc.	p.a. (deg)		Obs. Time (min.)	Flux Density (mJy)	perc.	p.a. (deg)	
1004+13	4C 13.41 PKS	10 04 45.05	+13 03 37.7				18720 (72 m)	579±30	4.1±1.6	50±22	115±2	17.2	117±2	6x15 (72 m)	127±462	6.4±0.9	37±8			6x15 (72 m)	127±462	6.4±0.9	37±8	0.240		
1011+23	4C 23.25 PKS	10 11 59.29	+23 16 04.2				6x15 (72 m)	205±12	6.2±0.8	49±6	30±5	10±6	100±8	6x15 (72 m)	49±25	10.7±0.7	22±4			6x15 (72 m)	49±25	10.7±0.7	22±4	0.365		
1012+48	4C 48.28	10 12 50.01	+48 52 56.8				18720 (72 m)	160±8	7.1±2.6	110±20	109±1	13.7	6.3±0.5	18720 (72 m)	560±30	10±2	16±12			18720 (72 m)	560±30	10±2	16±12	0.385		
1023+06	3C 243 PKS	10 23 55.13	+06 42 50.5				6x15 (72 m)	205	27±22	7.8±2.3	92±17	1.28	0.9	15±10	380±19	11.0±0.6	150±3			6x15 (72 m)	380±19	11.0±0.6	150±3	1.499		
1046+05	4C 05.46	10 46 56.63	+05 21 25.6				6x15 (72 m)	75	10±25	480	8.5±2.0	1.3	110±40												1.115	
1047+09	4C 09.37	10 47 48.95	+09 41 47.7				18720 (72 m)	166±7	5.1	51	71±2	10.4	119±3	5x15 (72 m)	384±38	4.30	50±20			5x15 (72 m)	384±38	4.30	50±20	0.786		
1048-09	3C 246 PKS	10 48 59.42	-09 02 13.2				6x15 (72 m)	30	38±2	4.30	83±3	11.8	122±4	6x15 (72 m)	1700±90	3.4±1.2	50±20			6x15 (72 m)	1700±90	3.4±1.2	50±20	0.344		
1055+20	4C 20.24 PKS	10 55 37.59	+20 07 55.3				18720 (72 m)	612	68±34	2.9±0.5	116±10			18720 (72 m)	688±34	2.9±0.5	116±10			18720 (72 m)	688±34	2.9±0.5	116±10	1.110		
1058+11	4C 10.30	10 58 10.80	+11 02 19.4				18720 (72 m)	512	205±12	9.6±3.7	32±2	31±1	5.2	92±10											0.420	
1105+77	3C 74.9 4C 77.09	11 00 27.32	+77 15 08.6				18720 (72 m)	71	87±5	19.6±2.0	11±6	6±30		18720 (72 m)	96±6	4.9	90±40			18720 (72 m)	96±6	4.9	90±40	0.311		
1111+40	3C 254 4C 40.28	11 11 53.35	+40 53 42.0				6x15 (72 m)	300	320±16	8.0±1.5	107±11			6x15 (72 m)	83±42	2.0	105±7			6x15 (72 m)	83±42	2.0	105±7	0.734		
1123+30	3C 261 4C 30.22 B2	11 32 16.76	+30 22 01.5				6x15 (72 m)	132	31±18	4.17	8.3±1.6	1.1	138±10	6x15 (72 m)	96±6	4.9	90±40			6x15 (72 m)	96±6	4.9	90±40	0.614		
1136-13	PKS	11 36 38.31	-13 34 05.9				6x15 (72 m)	166±9	237±111	4.4	9±2	1.4	104±25												0.554	
1137+66	3C 263 4C 66.13	11 37 09.30	+66 04 27.0				18720 (72 m)	750±37	100±60	3	66±1	7.6	112±1	18720 (72 m)	291±58	4.7	100±27			18720 (72 m)	291±58	4.7	100±27	0.652		
1150+49	4C 49.22	11 50 43.98	+49 47 49.3				6x15 (72 m)	1031	141±671	4.3±0.6	107±6	6.5±1.0	1.1	75±12											0.334	
1203+10	4C 10.34	12 03 22.34	+10 59 35.1				18720 (72 m)	108±9	8.8±5.1	81±32	10±2	1.7	102±27												1.088	
1206+43	3C 268.4 4C 43.13	12 06 42.16	+43 56 02.6				6x15 (72 m)	123	107±7	2.9±1.2	83±23	9±1	1.2	47±8											1.400	
1217+02	PKS	12 17 38.35	+02 20 22.42				6x30 (72 m)	120	162±8	4.2±2.2	130±8			6x30 (72 m)	669	73±36	1.3±0.5	65±19			6x30 (72 m)	669	73±36	1.3±0.5	65±19	0.240
1218+33	PKS 4C 33.29 B2	12 18 04.00	+33 59 50.0				6x15 (72 m)	710	905±50	13±1	93±4	7±2	0.7	165±10							6x15 (72 m)	905±50	13±1	93±4	1.519	
1221+18	4C 18.34	12 21 14.61	+18 37 43.3				18720 (72 m)	62	73±7	12.1±2.6	41±12	23±2	3.2	126±6							18720 (72 m)	62	73±7	12.1±2.6	41±12	1.401

Table 3 (continued)

Source	Alt. Name	Position (1950)			DEC m s	Obs. Time (Min. Basel)	Flux Density (Jy)		Polarization		Extension			1414 MHz		610 MHz		Redshift
		R.A. h m s	d	BEC m s			Peak	Total	perc.	p.a. (deg)	arc sec	size	Fr. beam	p.a. (deg)	Flux Density (mJy)	Polarization perc.	p.a. (deg)	
1222-21	4C 21.35 PKS	12 22 23.39	+21 39 22.4		6415 (72 m)	<50	874±44	< 8		12±1	1.9	70±12						0.435
1223-25	4C 25.40 B2	12 23 09.11	+25 15 11.9		14720 (72 m)	579 215±20 90	675±34 103±5	2.8±0.8 < 8	129±16	67±2	7.1	31±1						0.265
1226-02	3C 273 PKS 4C 16.32	12 26 33.23	+02 19 42.9		6415 (72 m)	28 6 45	36±3 7±5 46±05±200	<15 7.2±2.3 < 1	109±17	9±6 16±6 21±0	3.0±1.5 3.0±1.0 2.3	42±10						0.158
1229-02	4C 01.55 PKS	12 29 25.88	-02 07 31.9		6415 (72 m)	2880 40080 51220	4300±200 41500±2100 897±44	<1.5 1.7±0.5 4.7±0.7	166±22	< 5 BM	u							1.038
1232-24	PKS	12 32 59.40	-24 55 44.3		9415 (72 m)	155 18 161	334±17 11±2 265±13	15.4±1.2 5.4±5	54±5	86±2	7.5	160±1						0.355
1241+16	3C 275.1 4C 16.34 PKS	12 41 27.57	+16 39 17.8		6415 (72 m)	808	107±54	< 6	104±15	14±3	0.8	160±5						0.557
1258+40	3C 280.1 4C 40.32	12 58 14.15	+40 25 15.4		14720 (72 m)	173 60 95	192±10 90±15 314±15	6.8±0.9 12.5±1.7	20±8	20±1	3.2	114±4						1.659
1305-06	3C 281 4C 06.45 PKS	13 05 22.48	+06 58 12.9		6415 (72 m)	175	185±11	< 9	32±22	36±3	3.0	158±2						0.528
1357-21	PKS	13 27 23.36	-21 26 33.8		3415 (72)	100 276 165	24±13 295±15 325±17	< 5 < 3										
1332+55	4C 55.27	13 32 15.83	+55 16 45.1		14720 (36 m)	44	53±4	9.1±3.2	153±20	76±1	11.4	141±1						1.21
1335-06	4C 06.35 PKS	13 35 31.18	-06 11 57.1		6415 (72 m)	6 37 424	6±2 48±3 908±45	<12 < 7		6±3	6	170±20						0.625
1354+19	4C 19.44 PKS	13 54 42.14	+19 33 42.6		6415 (72 m)	1330	1740±87	4.5±0.6	73±8	15±3	1.0	165±5						0.720
1422+20	4C 20.33 PKS	14 22 37.56	+20 13 57.4		6415 (72 m)	10(29)	610±21	< 10	72±7	11±3	0.6	0±5						0.871
1427+24	4C 24.31 PKS	14 23 34.86	+24 17 31.9		14720 (72 m)	140	192±10	3.7±1.2	85±19	18±2	2.1	29±4						(0.649)
1429-26	B2	14 25 21.88	+26 45 38.7		14720 (36 m)	270	352±16	6.5±0.7	113±6	5±3	31.5	56±3						0.366
1442+10	04 172	14 42 11.0	+10 11 18.4		5815 (72 m)	10(29) 58(60) 5(15)	78±5 60±4 20±10	<12 < 10 < 5		25±4 6±14 20±10	b	70±20						0.350
1449-01	4C 00.57 PKS	14 49 12.83	-01 15 18.4		8415	184	264±13	< 10	64±11	<4R	u							1.314
1511+09	4C 09.52 PKS	14 51 27.9	+09 46 33.0		6460 (72 m)	65	82±7	< 16		23±3	3.4	63±13						0.627

Table 3 (continued)

Source	Alt. Names	Position (J2000)			DBQ	Obs. Time (Min.)	995 MHz Flux Density (mJy)		Polarization		Extension			415 MHz Flux Density (mJy)		Polarization		Obs. Time (Min.)	410 MHz Flux Density (mJy)	Polarization	Redshift
		R.A. m s	Dec. d m s	Peak			Total	perc.	p.a. (deg)	arc-sec	size	n. beam	p.a. (deg)	perc.	p.a. (deg)	perc.	p.a. (deg)				
1653-10	PKS	14 53 12.10	-10 56 37.8			18720 (72 m)	1303445				4.15	2.6	16043							0.940	
1508-39	4C 10.39		+105			400	309115	9.2±1.7	38±11											1.833	
1308-05	4C 05.64	15 08 00.18	+10 41 21.3			5815 (72 m)	2283114	-0.5	24±19											1.191	
1318-37	4C 37.43	15 08 16.93	-05 31 48.8			4915 (72 m)	2187109	3.3±0.6	7±10											0.371	
1542-37	4C 37.45	15 12 46.97	+37 01 55.1			1720 (72 m)	328416	5.5±2.2	14±23											0.972	
1543-21	4C 21.45	15 45 31.18	+21 01 27.5			18720 (72 m)	823541	5.8±1.0	133±10											0.264	
1548-02	PKS					165	278222													0.555	
1548-02	PKS					62	1064													0.713	
1618-17	4C 17.68	16 18 07.29	+17 43 30.2			3815 (72 m)	1195	1364±68	3.2±0.7	94±11										0.927	
1623-23	4C 23.43	16 22 32.45	+23 52 00.6			228	328425	13.8±1.6	57±7											1.254	
1628-36	4C 36.28	16 28 57.67	+36 19 30.9			145	150520	11.9±2.5	70±12											0.361	
1634-26	4C 34.26	16 34 34.22	+26 54 10.0			250	324216	6.8±0.7	160											0.371	
1704-60	4C 60.24	17 04 01.39	+60 48 31.3			419	17239	7.3±0.6	126											0.989	
1711-27	4C 27.38	17 41 00.0	+27 54 42.0			61	844													1.460	
2005-04	4C 04.76	20 05 46.33	-04 27 17.2			65	834													1.805	
2059-03	PKS					50	634													0.986	
2100-16	4C 16.72	21 00 25.52	+16 31 45.7			25	147													0.200	
2128-08	4C 08.62	21 28 54.57	+08 59 18.8			297	324214	6.5±0.5	133±4											0.464	
2135-14	PKS					28	3842													1.981	
2209-08	4C 08.64	22 09 32.24	+08 04 26.4			18	1872													0.323	
2225-05	4C 05.93	22 25 54.02	-05 34 16.6			632	96549	1.4±0.5	81±20											0.543	
2231-11	PKS					319	38519	4.5±1.4	100±18											0.420	
2232-12	PKS					215	38019	<1.1	149											0.896	
2233-11	PKS					237±42														1.460	
2234-12	PKS					573	6342													1.805	
2235-14	PKS					129	21631	5.6±1.1	171±11											0.986	
2235-16	PKS					327	34217													0.200	
2235-26	PKS					192	695470	15±5	16±22											0.464	
2235-26	PKS					80	97410													1.981	
2235-26	PKS					42	354470	5±2	71±20											0.323	
2235-26	PKS					970	97849	5.7±0.7	84±7											0.464	
2235-26	PKS					<1.5														1.981	
2235-26	PKS					6820														0.323	
2235-26	PKS					200411														1.460	
2235-26	PKS					362418														1.805	
2235-26	PKS					700	71326	2.9±0.7	135±14											0.986	
2235-26	PKS					6825	260113	<2.0												0.200	
2235-26	PKS					32	120510													0.464	
2235-26	PKS					55	132415													1.981	
2235-26	PKS					386	444422	5.0±0.8	51±9											0.323	
2235-26	PKS					223±20														0.464	
2235-26	PKS					38219														1.981	
2235-26	PKS					112	15048	6.3±1.1	172±10											0.323	
2235-26	PKS					10	2642													0.464	
2235-26	PKS					185	200110													1.981	
2235-26	PKS					3645	385192	<1.3												0.323	
2235-26	PKS					277	38519	6.8±1.7	24±10											0.464	
2235-26	PKS					<1.5														1.981	
2235-26	PKS					230450														0.323	



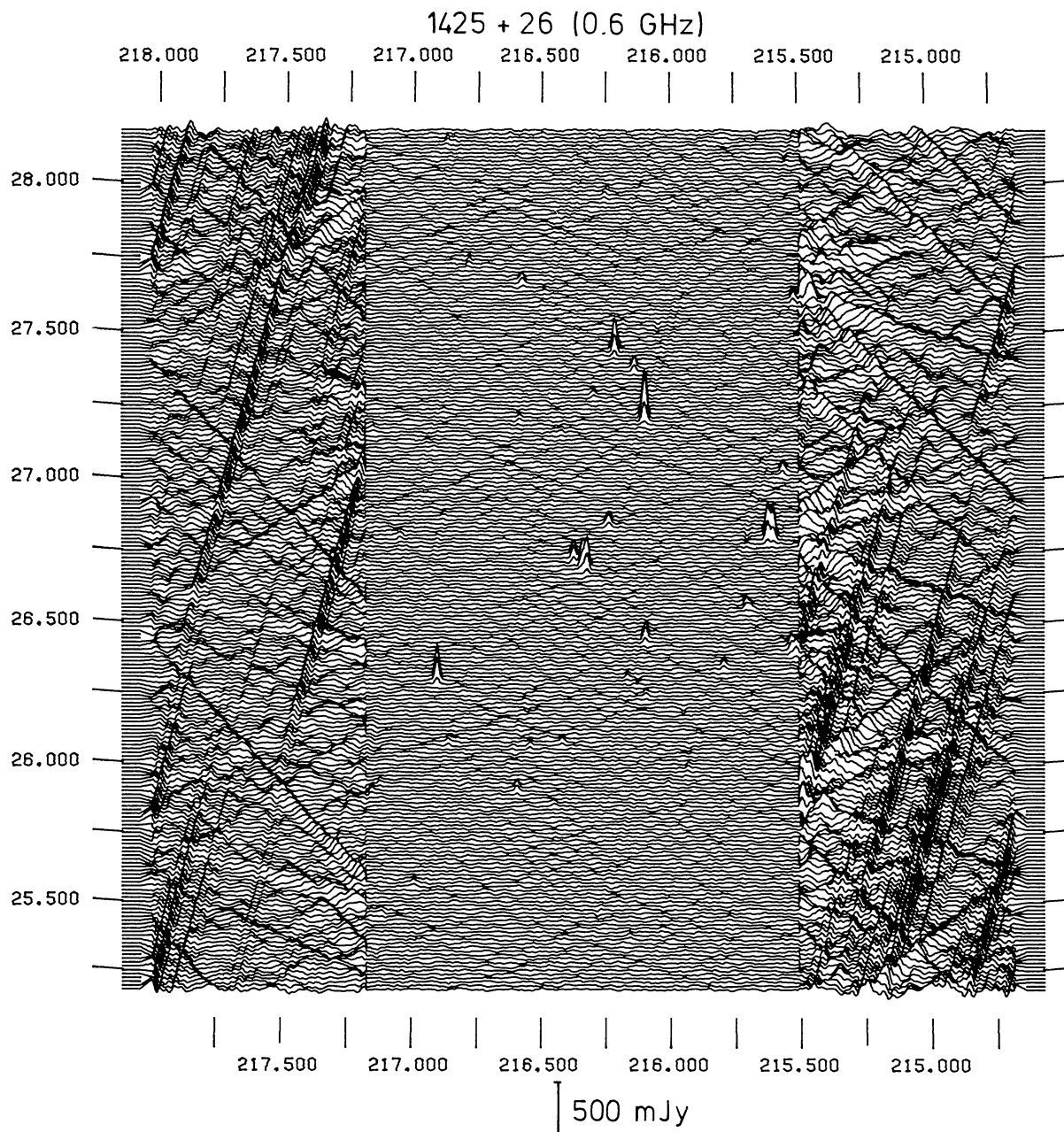


Figure 1 A profile plot of the  $3^\circ$  field surrounding 1425+26. This is the result of 6 fifteen minute observations at 610 MHz. A 512 by 512 transform was chosen to give a  $3^\circ$  by  $3^\circ$  cosec  $\delta$  field and the central 256 by 256 region was treated using the clean algorithm. Right ascension and declination are in decimal degrees referenced to epoch 1950.

Figure 2 The structures of all sources larger than 2.5 half power beam lengths. Unless otherwise indicated the frequency is 4995 MHz. The maps of total intensity and (where the signal to noise ratio is sufficient) of polarized intensity are shown as contour diagrams. The primary contour interval in mJy per beam area is indicated on the top right corner of each contour diagram and any additional contour levels used are shown at the top left corner. For the polarized intensities the vectors are superimposed on the contour maps. All declination scales are compressed to give effectively circular beams (shaped circles). The cross shows the position of the optical qso. The right ascensions and declinations are referenced to epoch 1950.

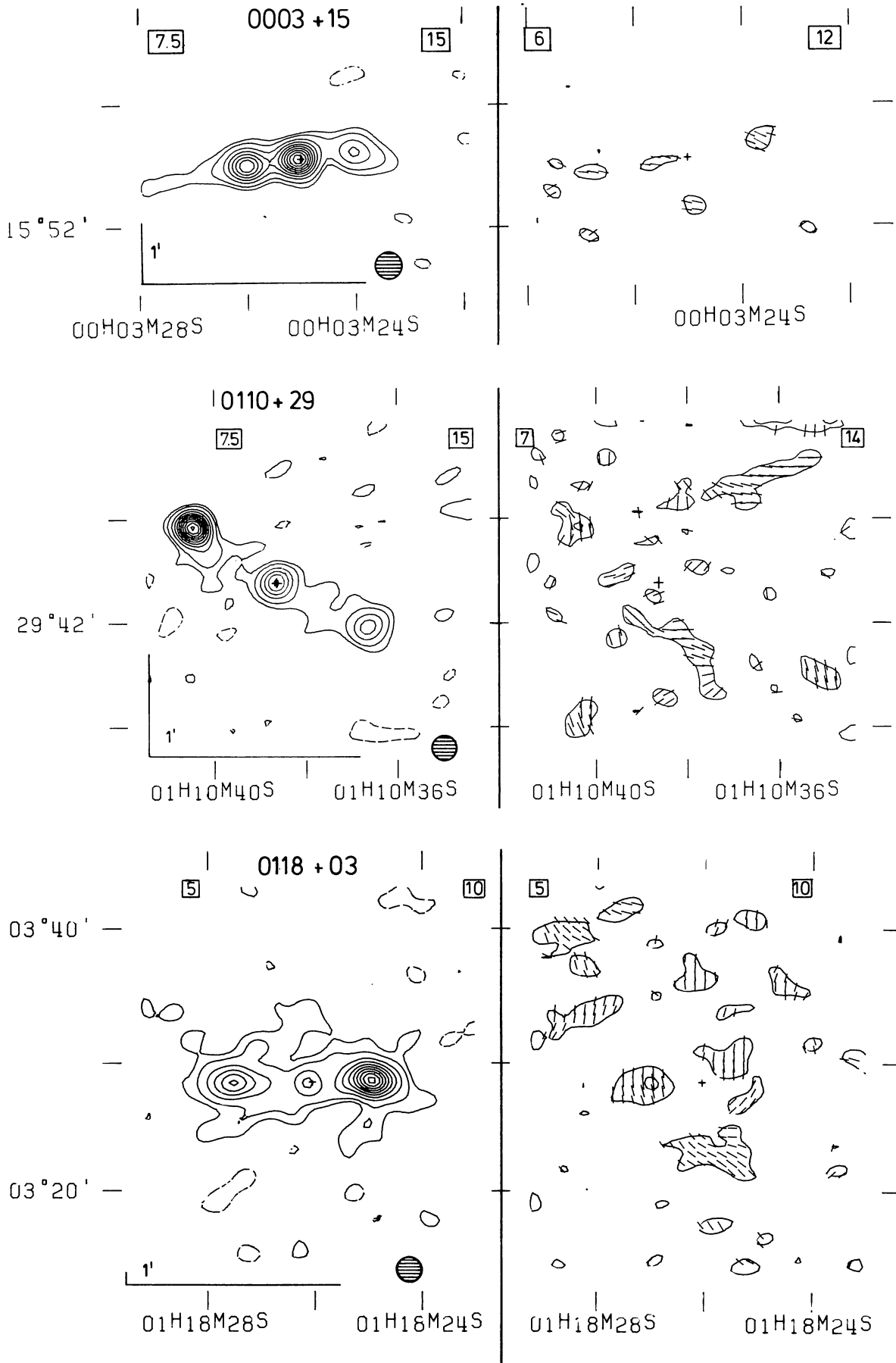


Figure 2

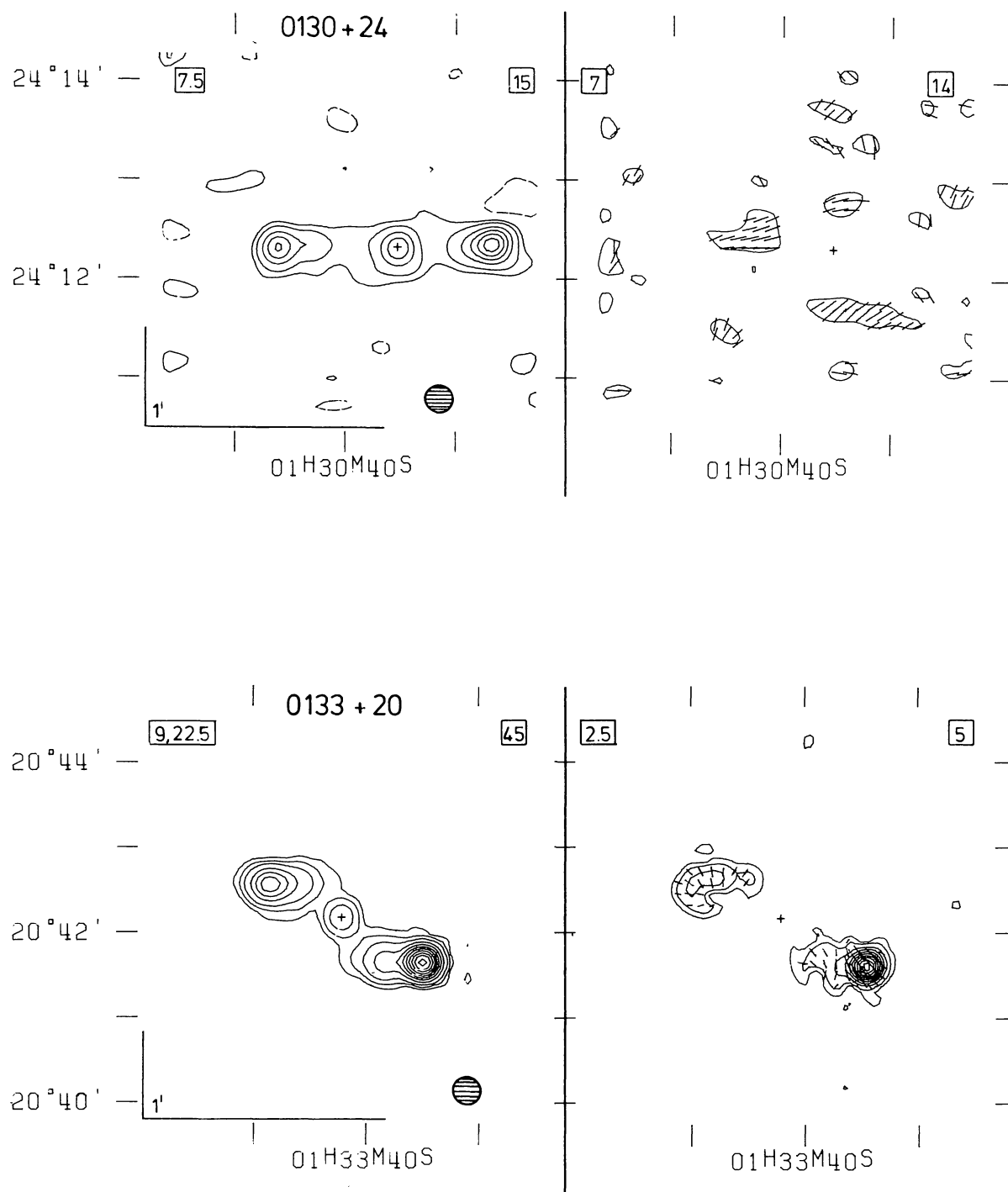


Figure 2 (continued)

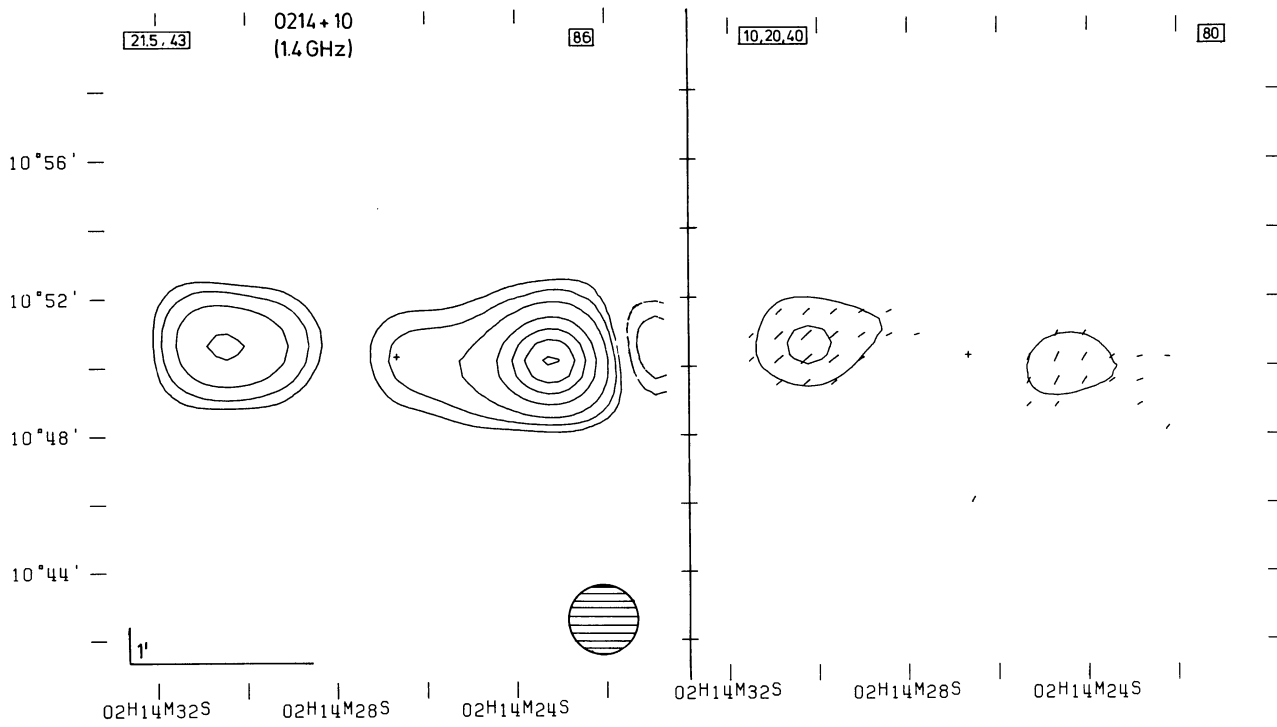
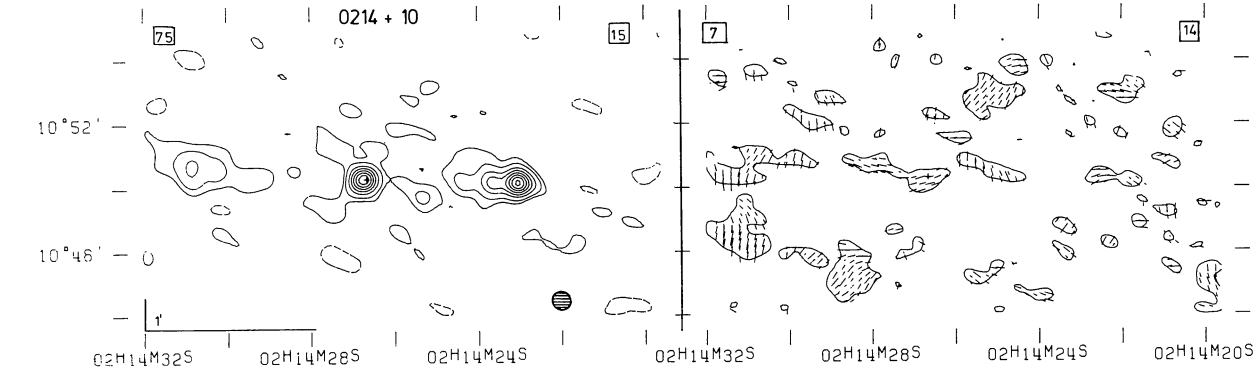


Figure 2 (continued)

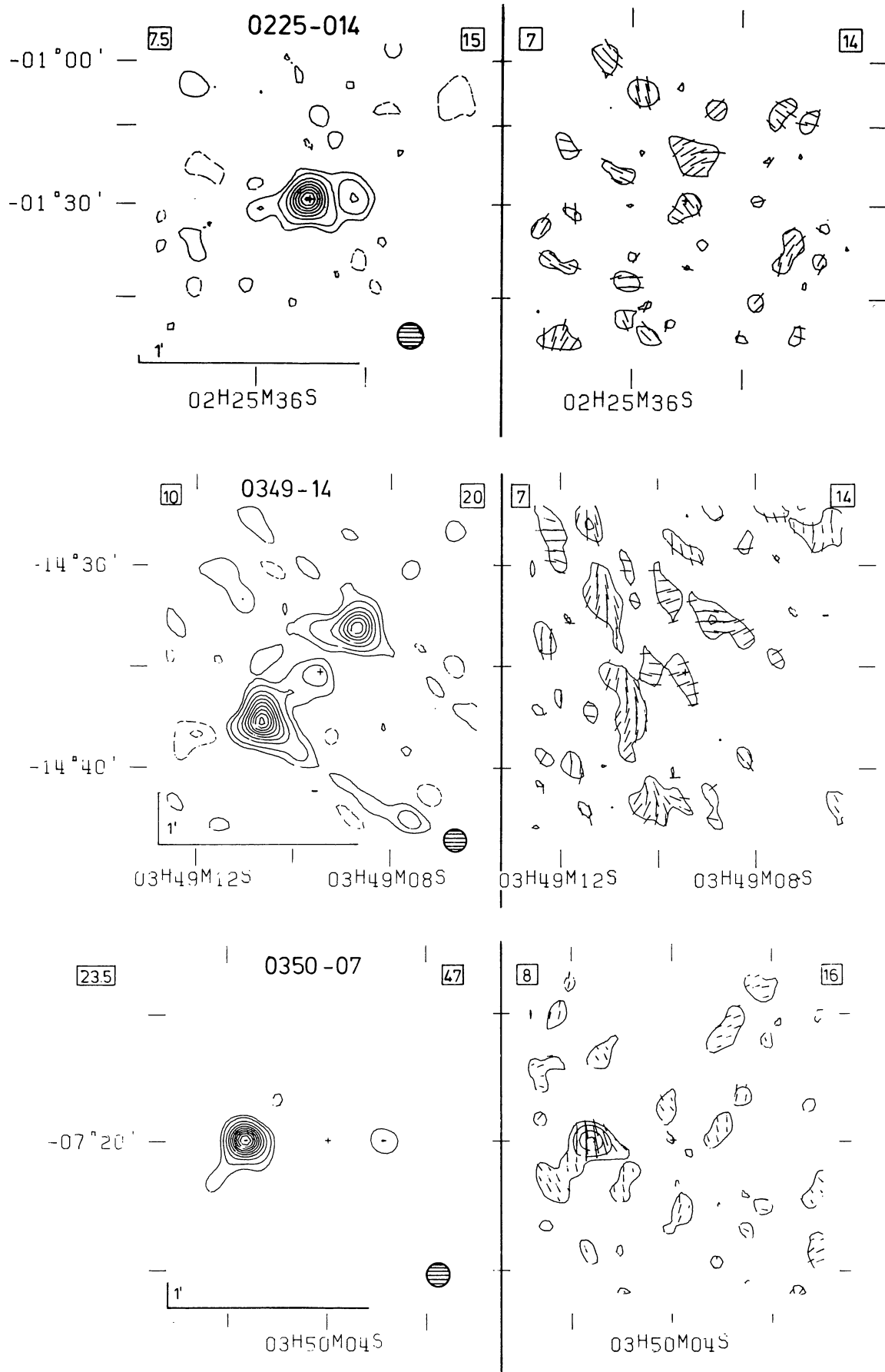


Figure 2 (continued)



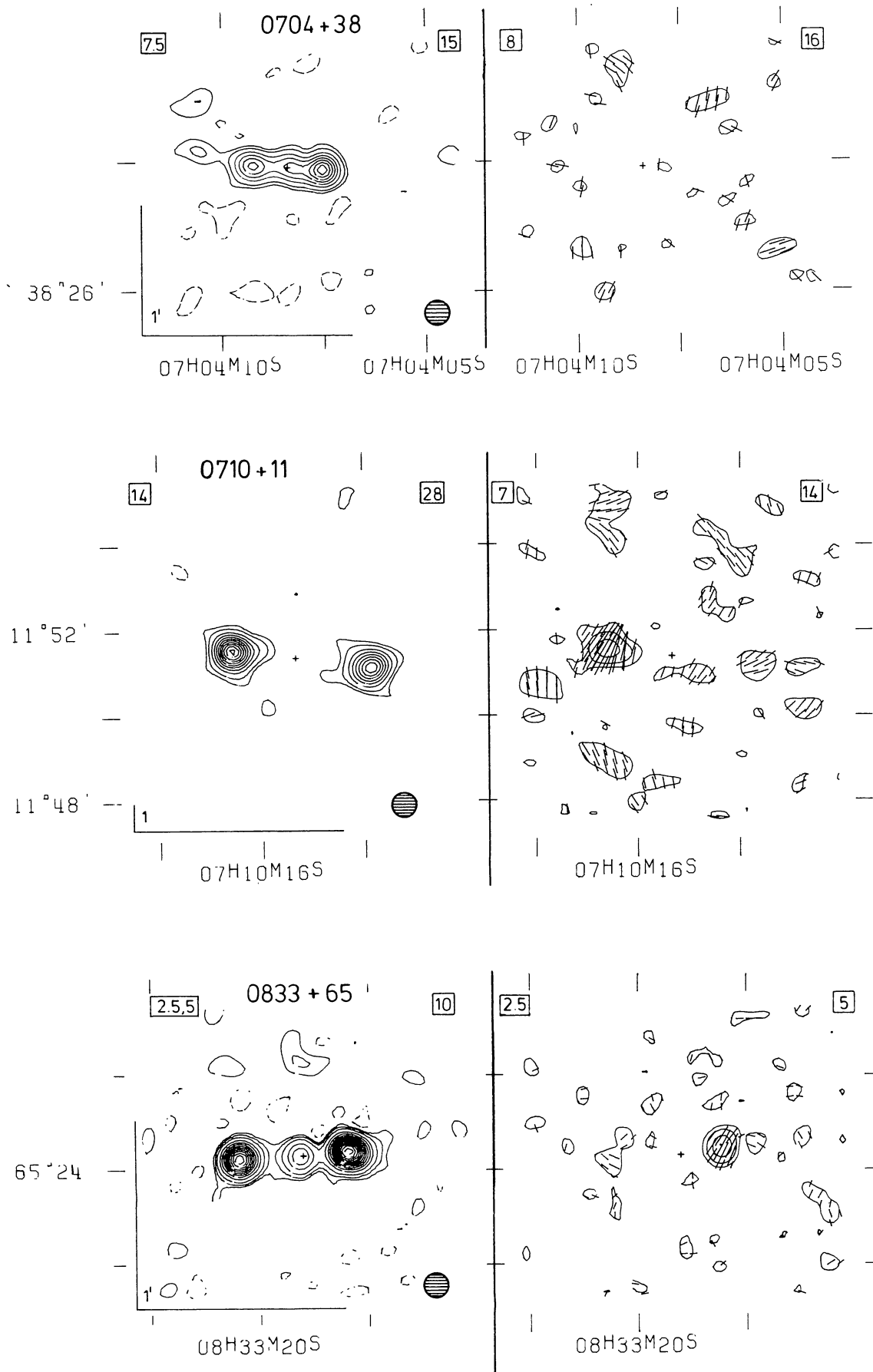


Figure 2 (continued)

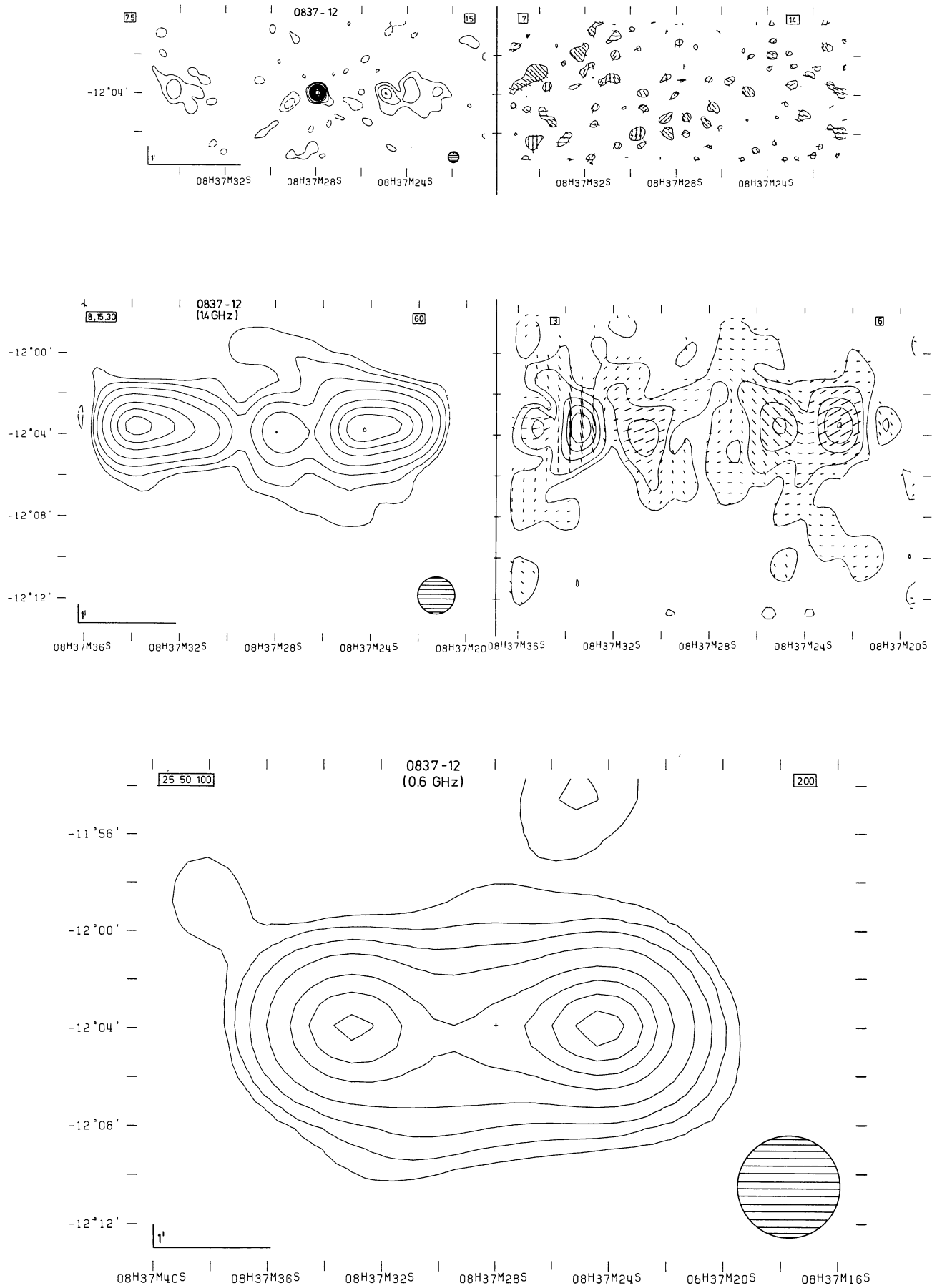


Figure 2 (continued)

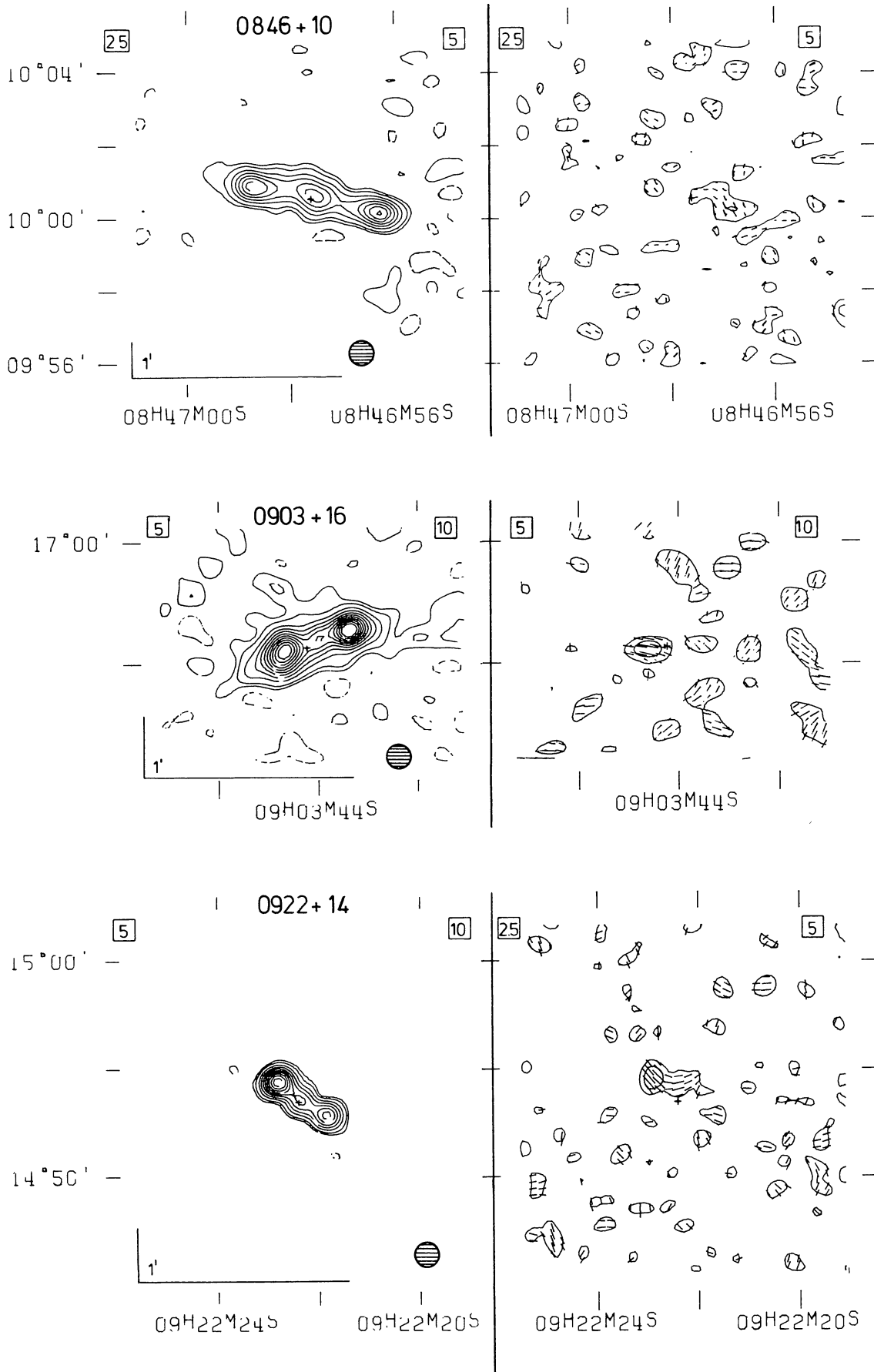


Figure 2 (continued)

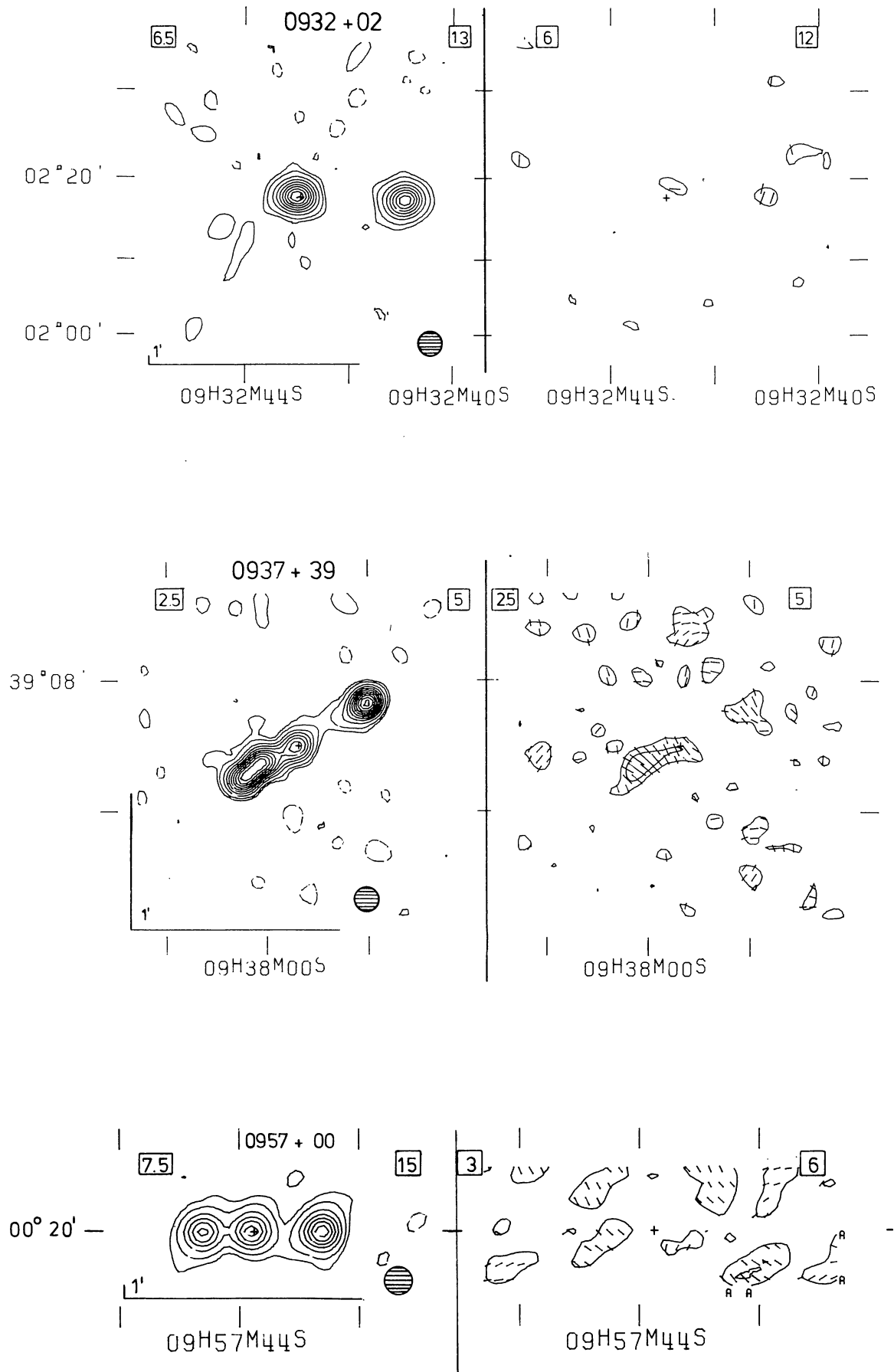


Figure 2 (continued)

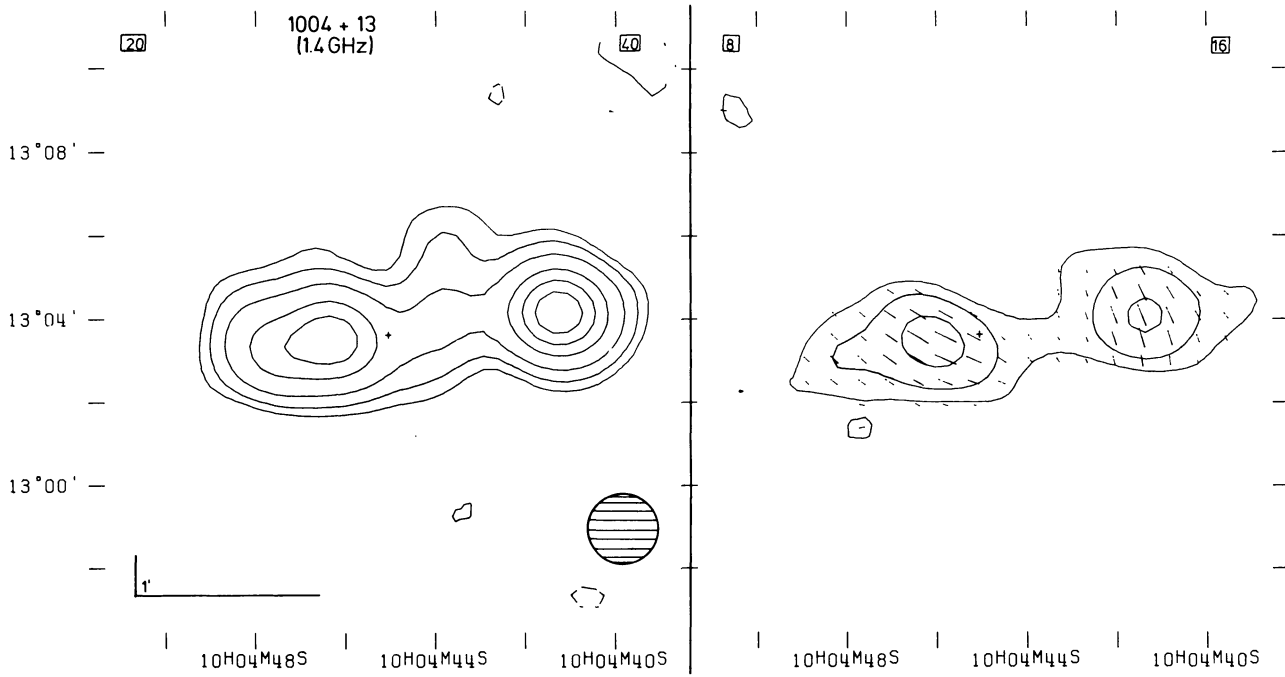
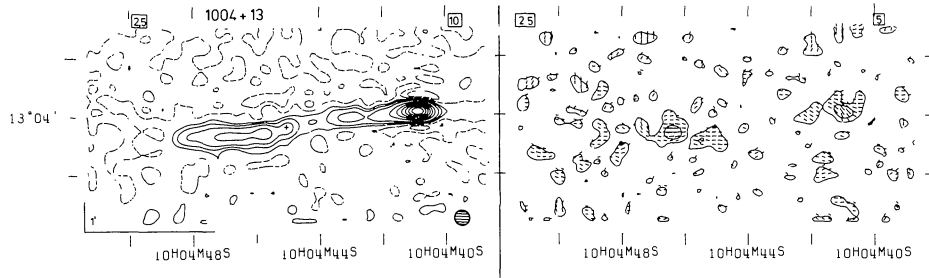


Figure 2 (continued)



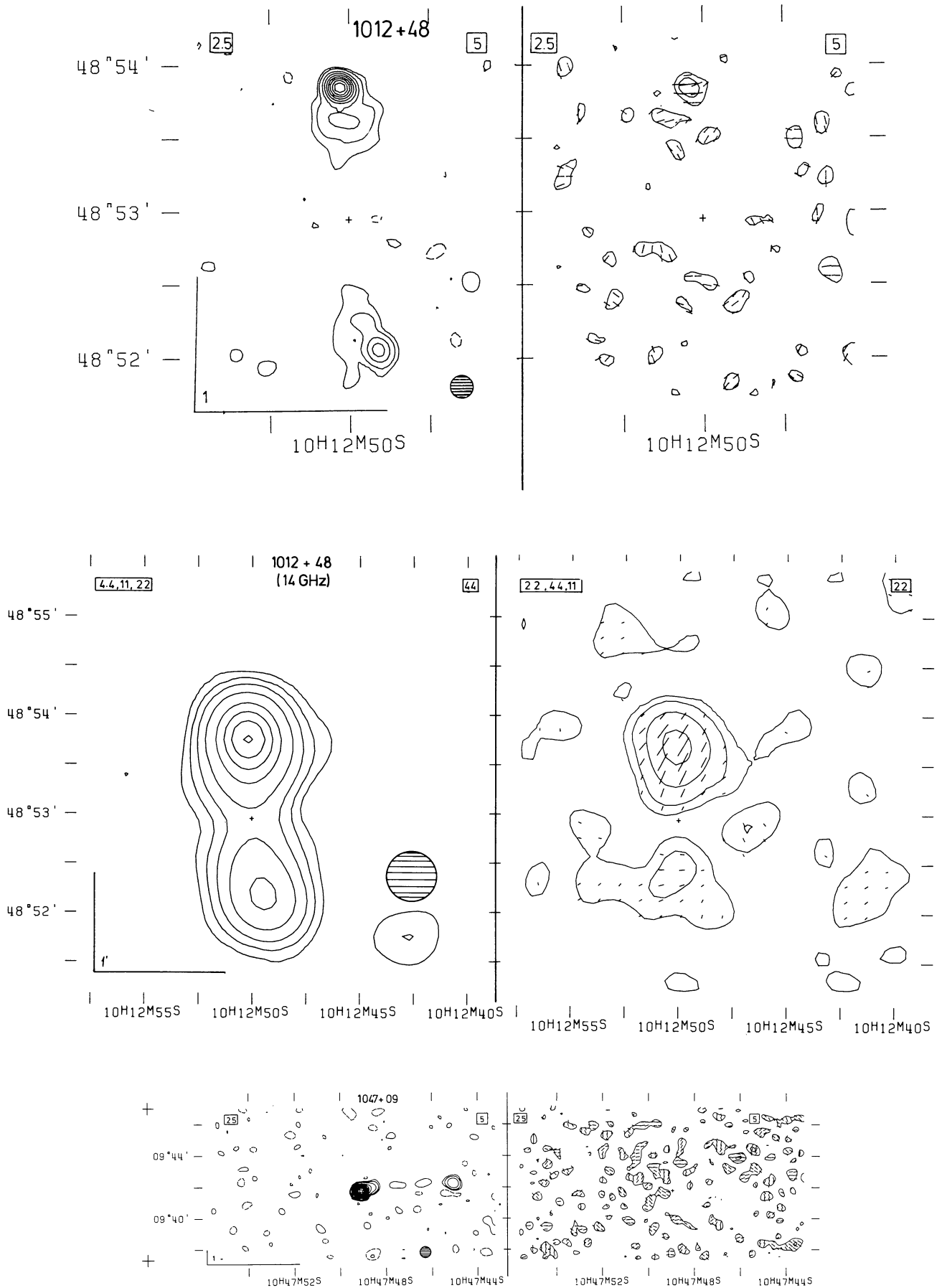


Figure 2 (continued)

1978AEAS...34..129M

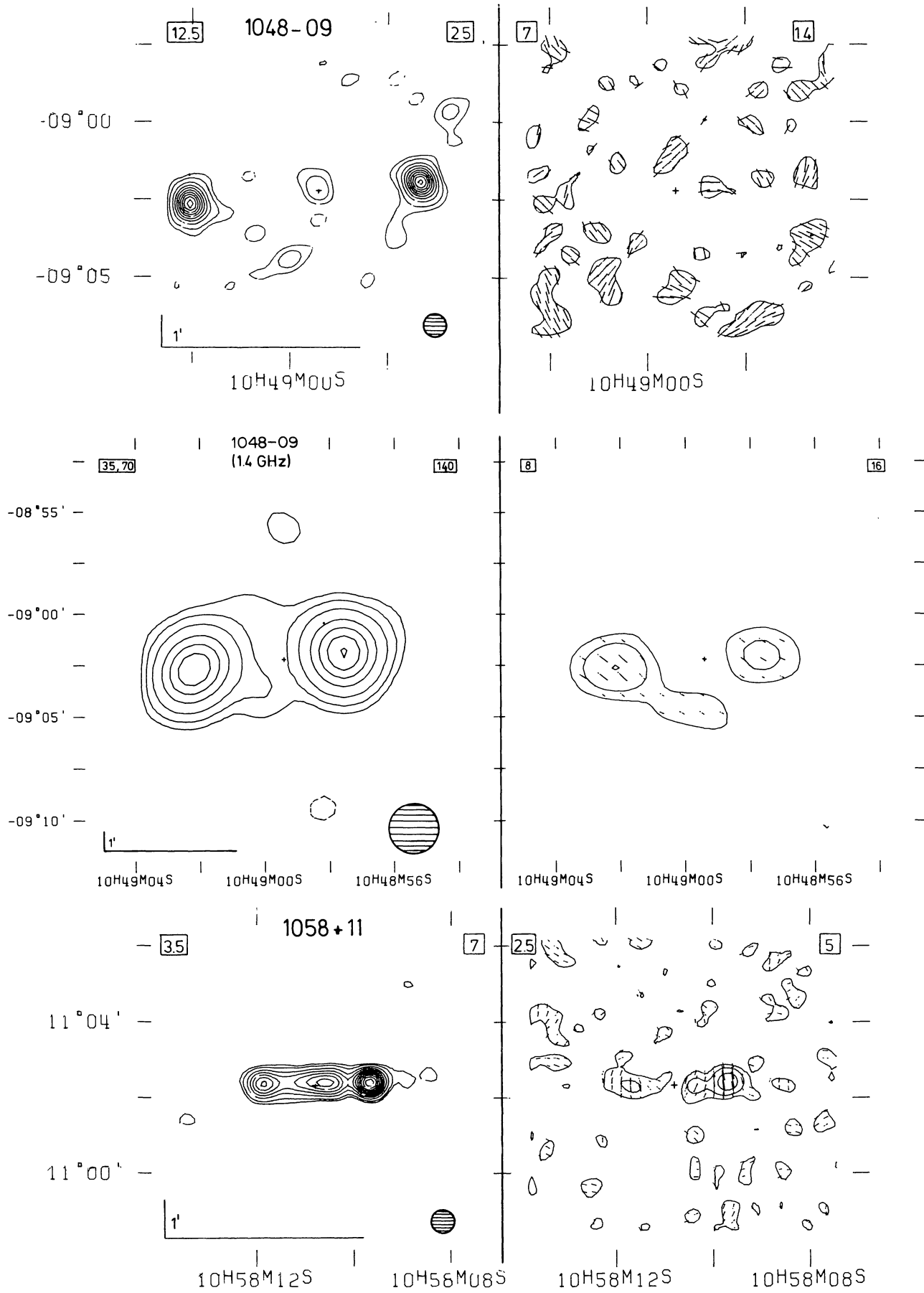


Figure 2 (continued)

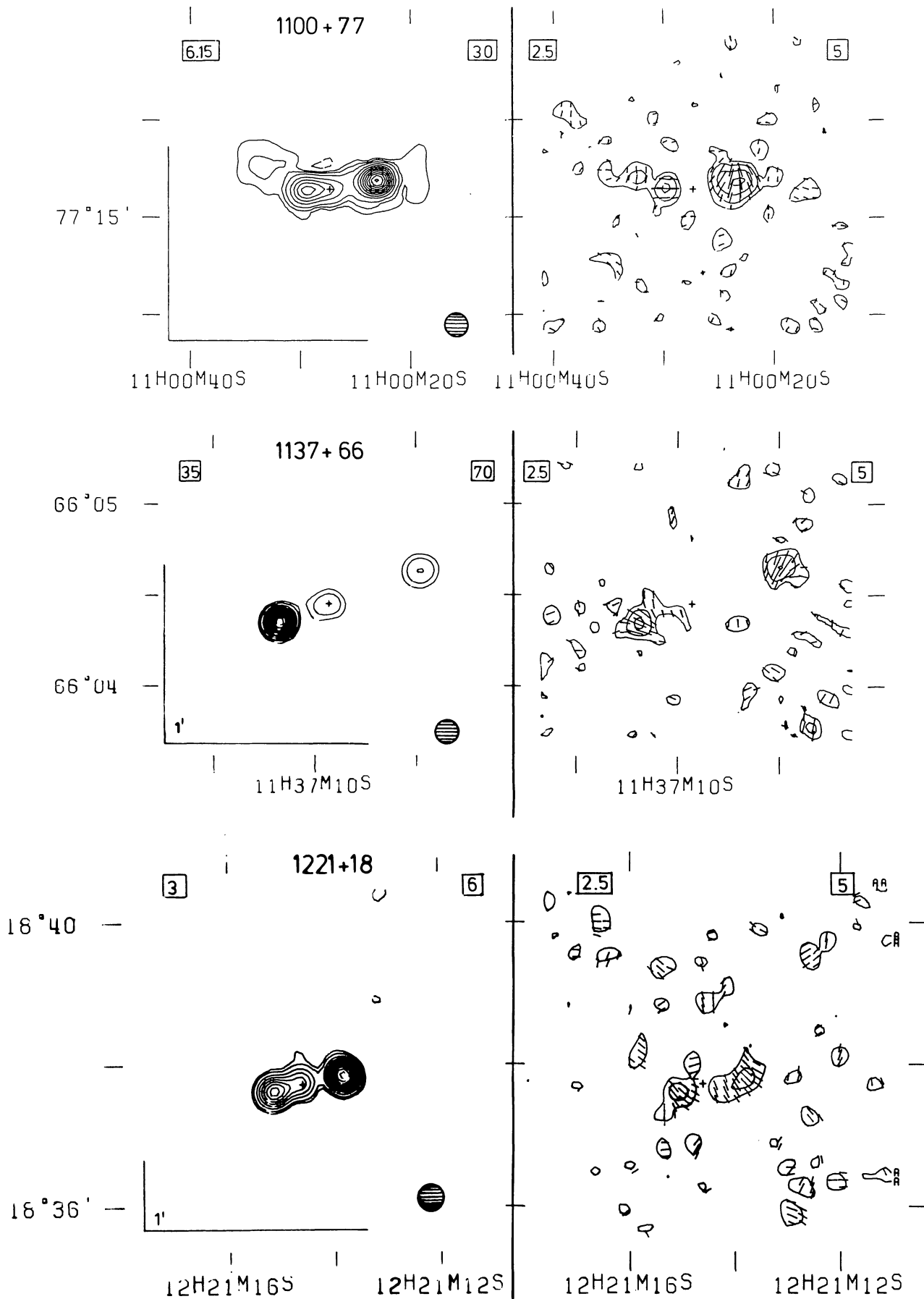


Figure 2 (continued)

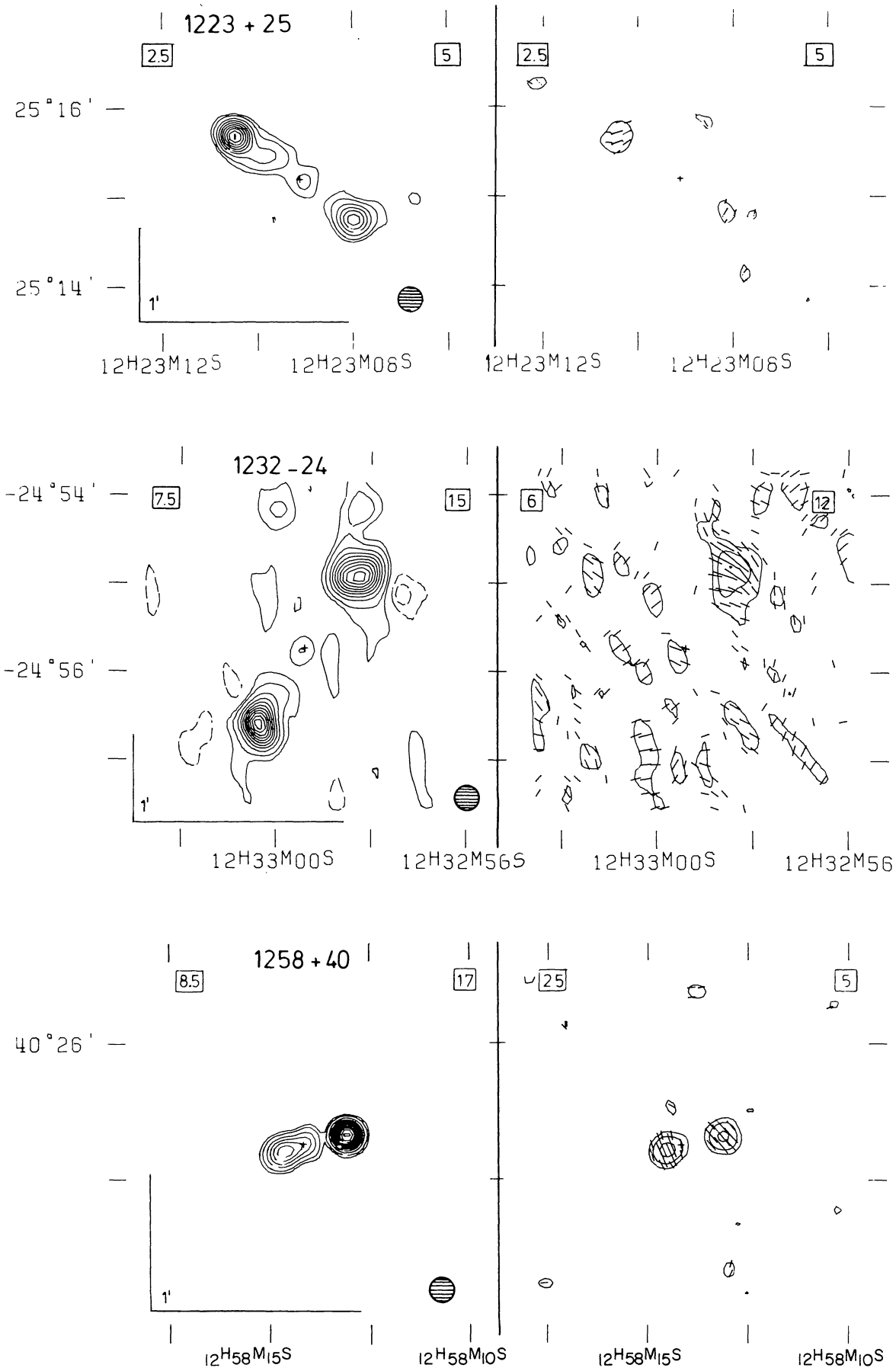


Figure 2 (continued)

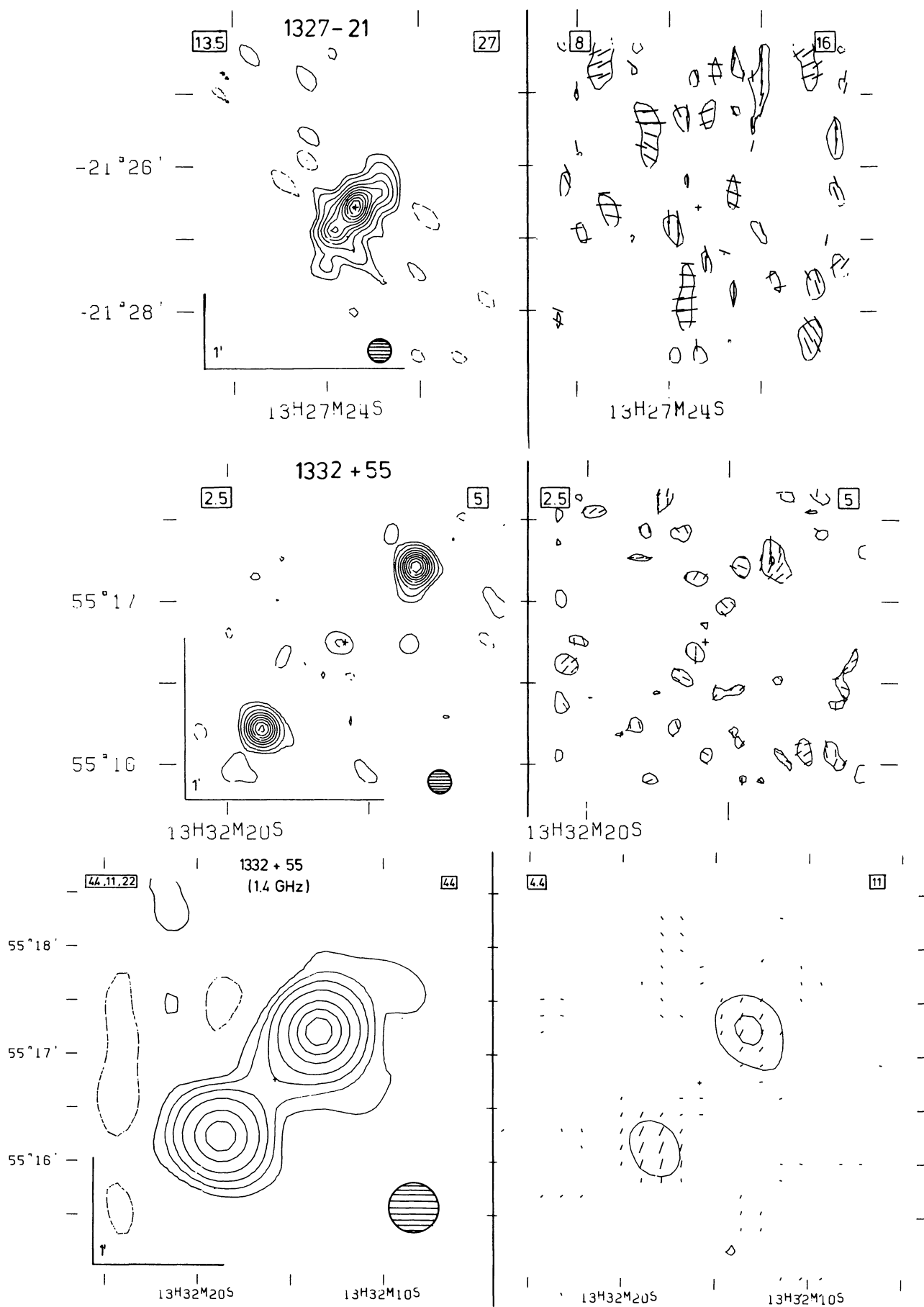


Figure 2 (continued)



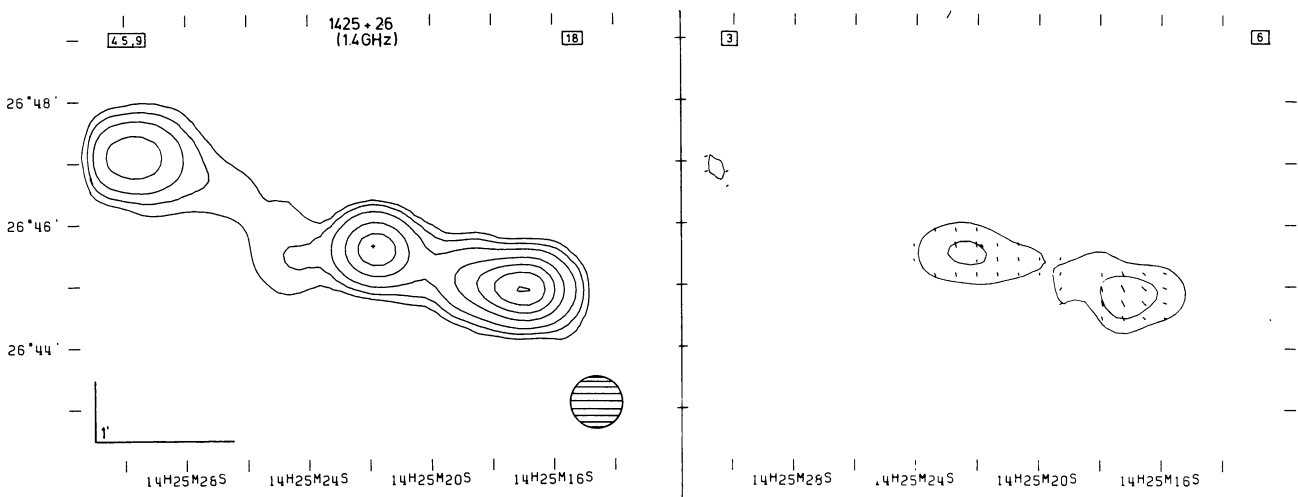
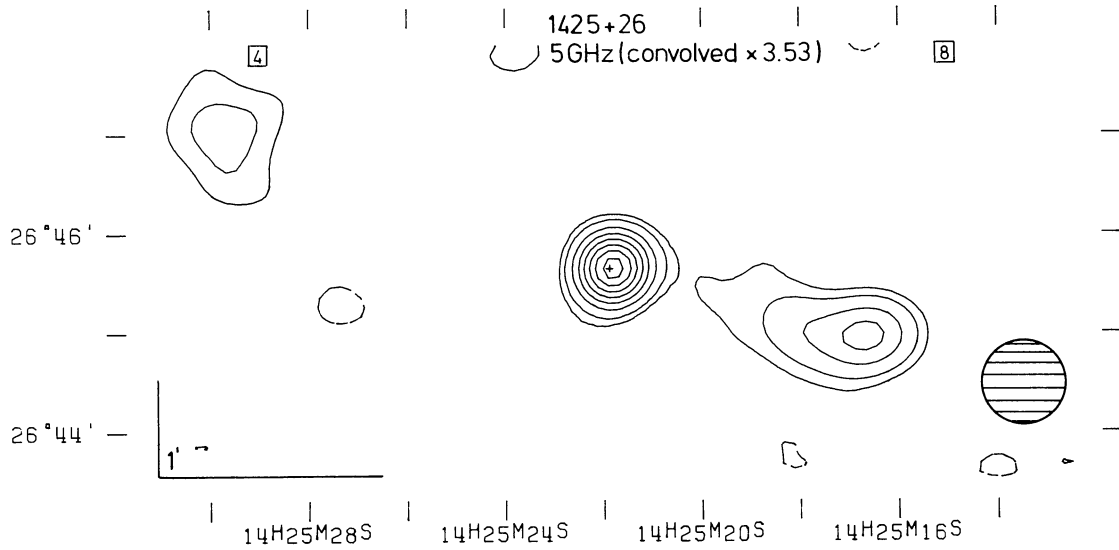
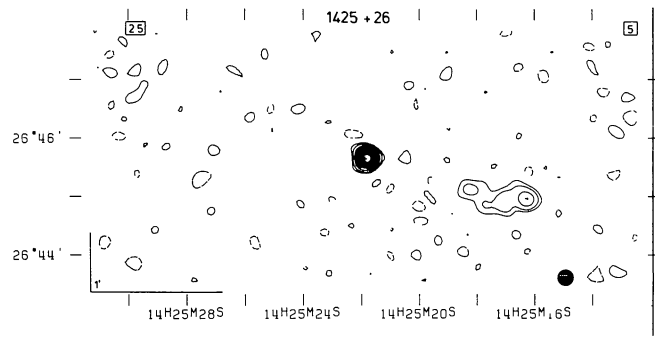


Figure 2 (continued)

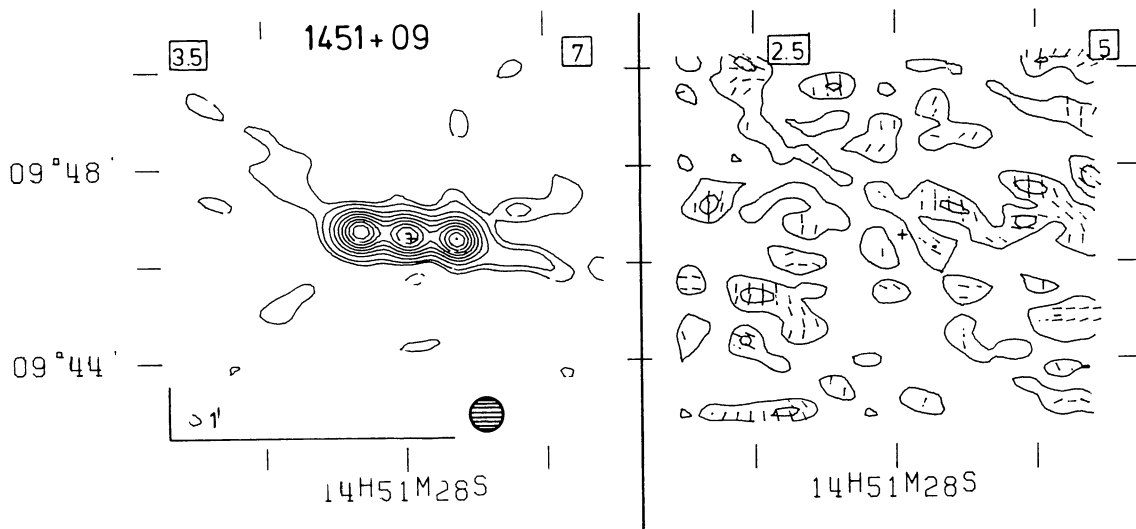
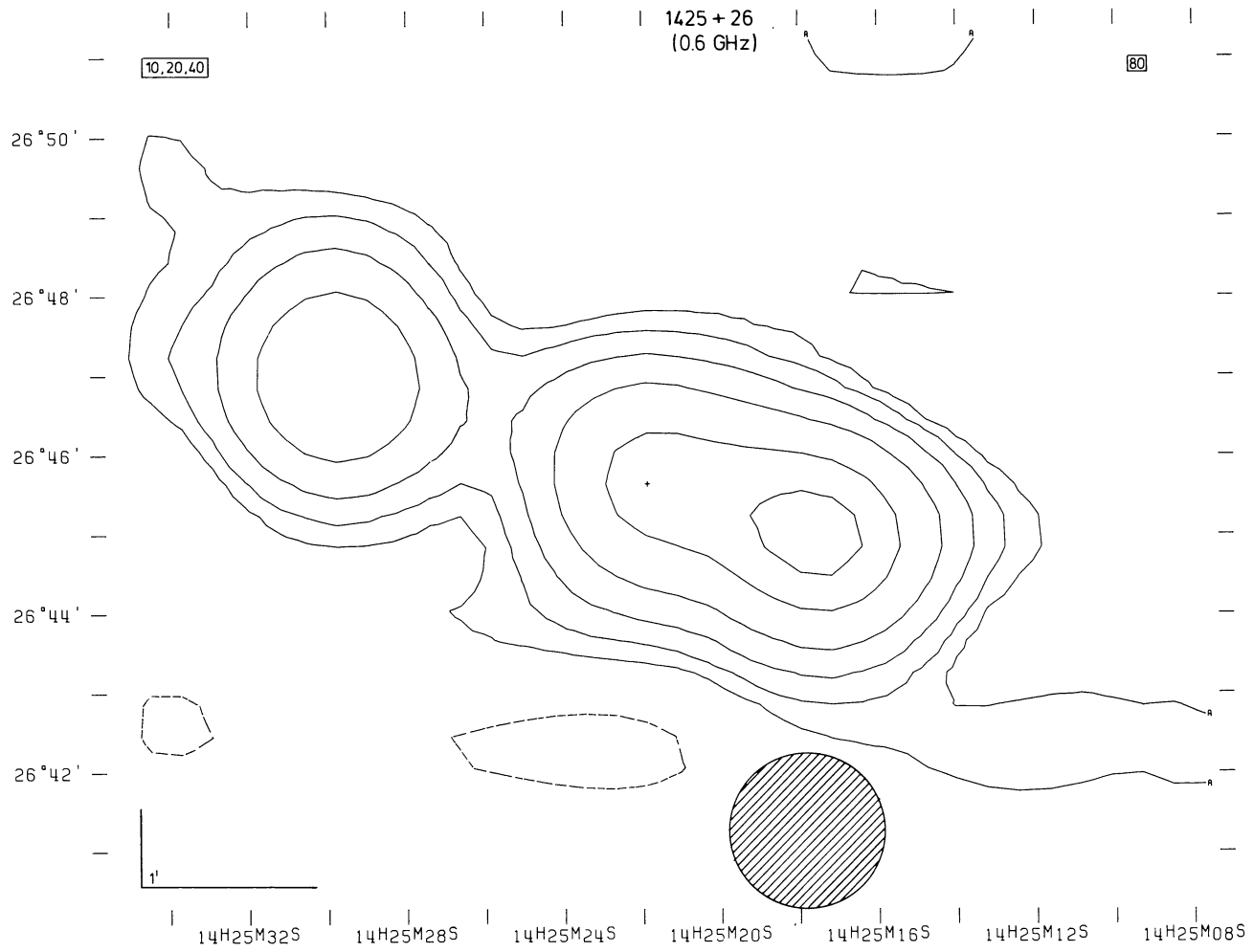


Figure 2 (continued)

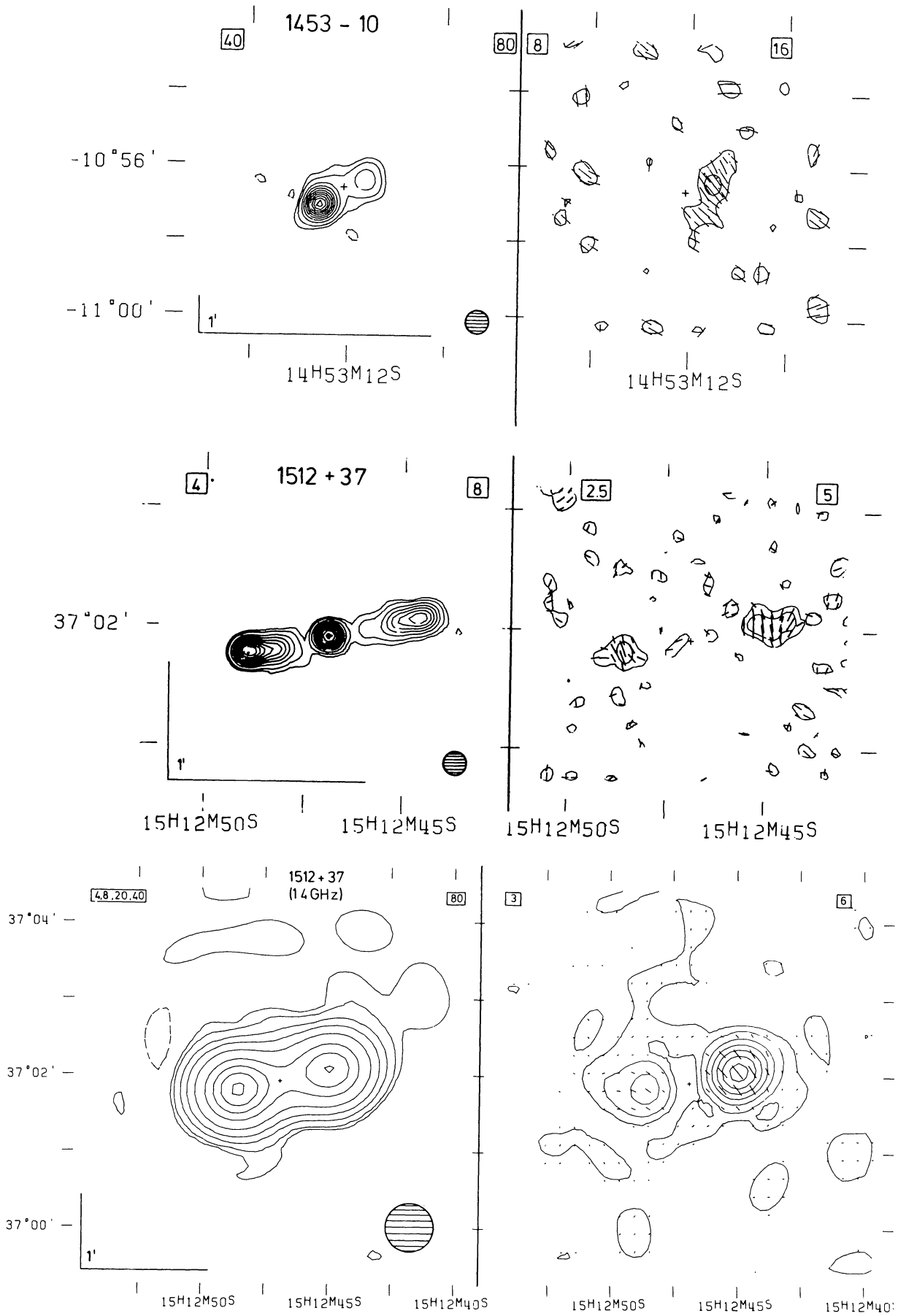


Figure 2 (continued)

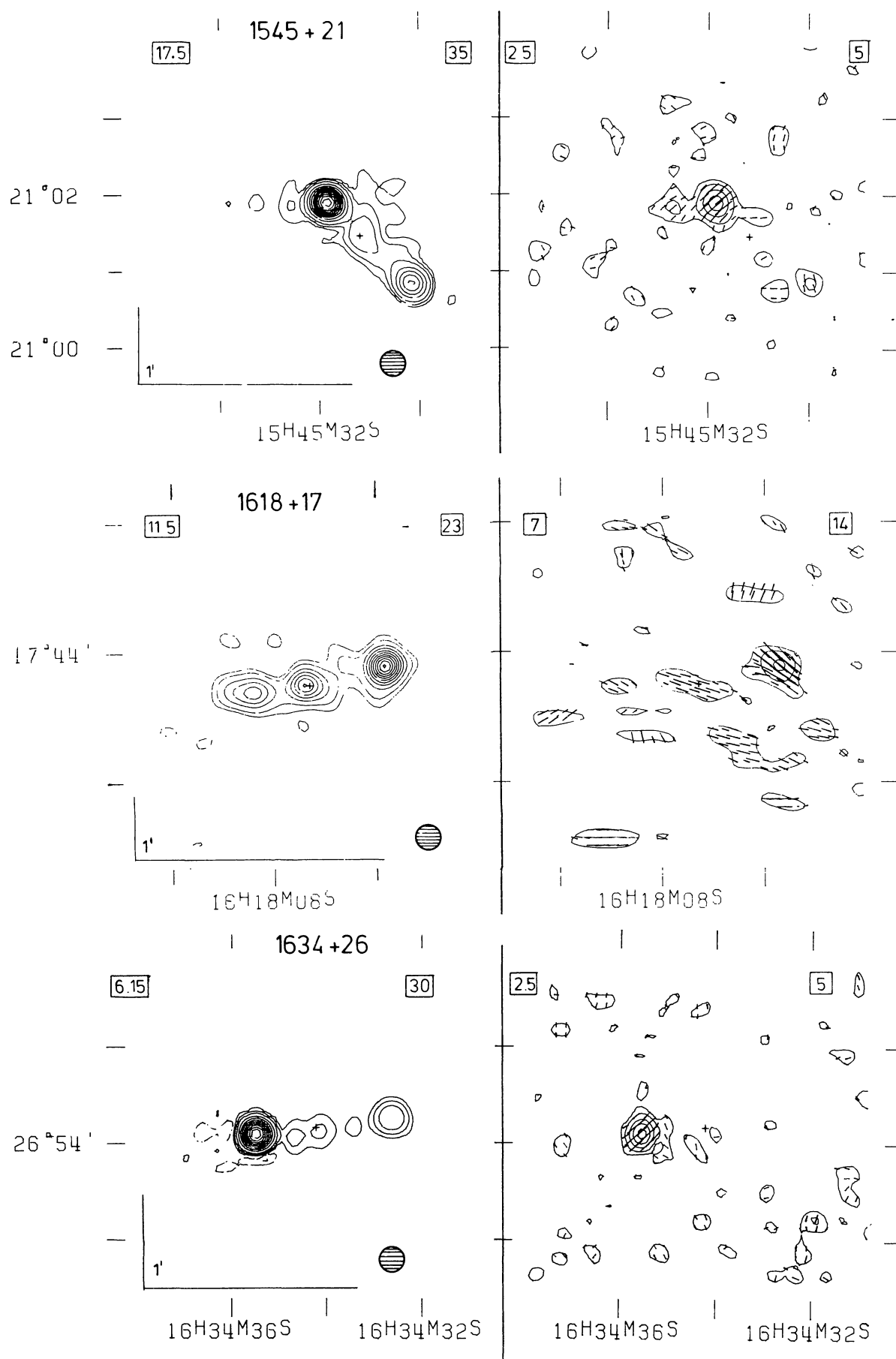


Figure 2 (continued)

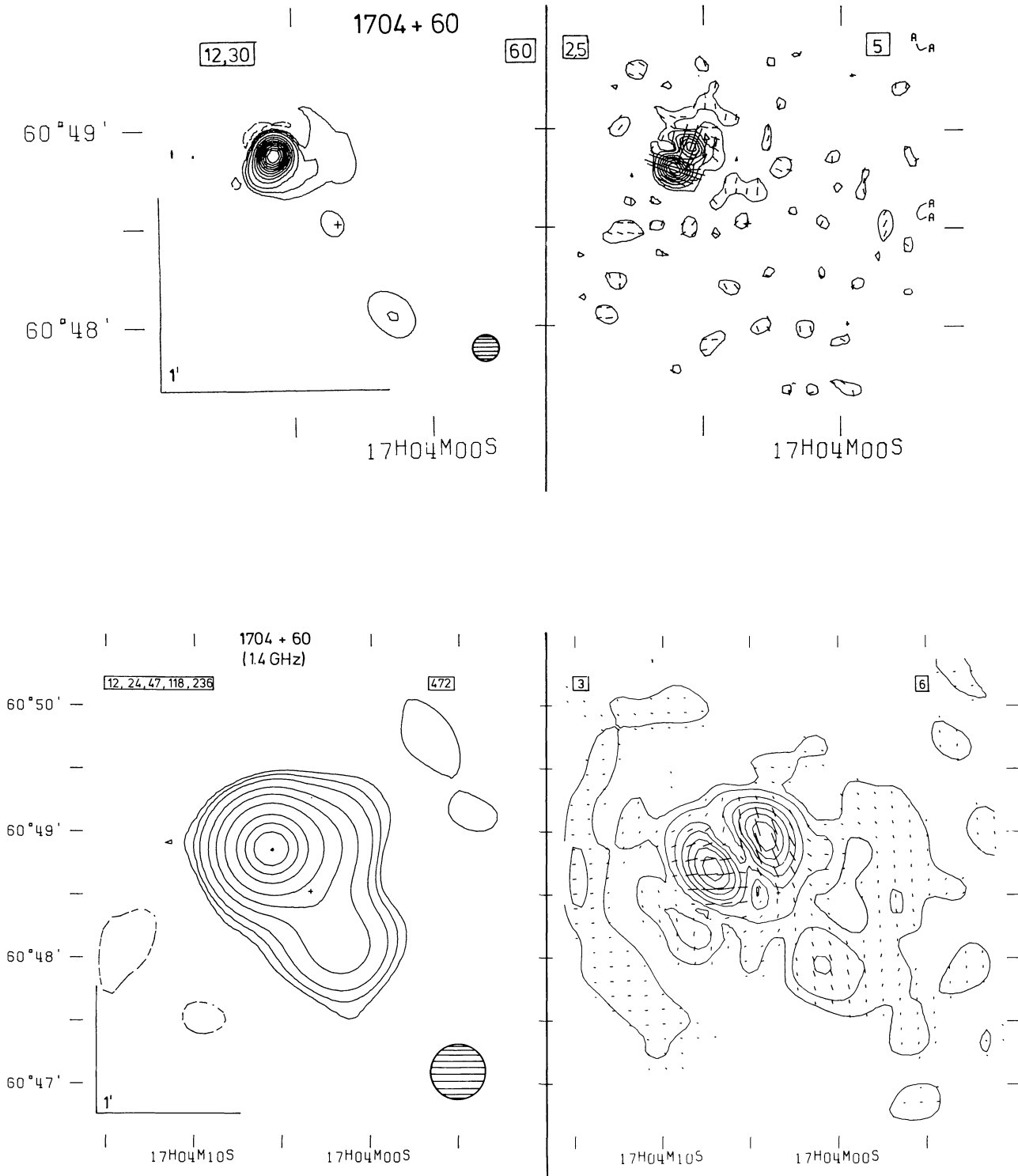


Figure 2 (continued)

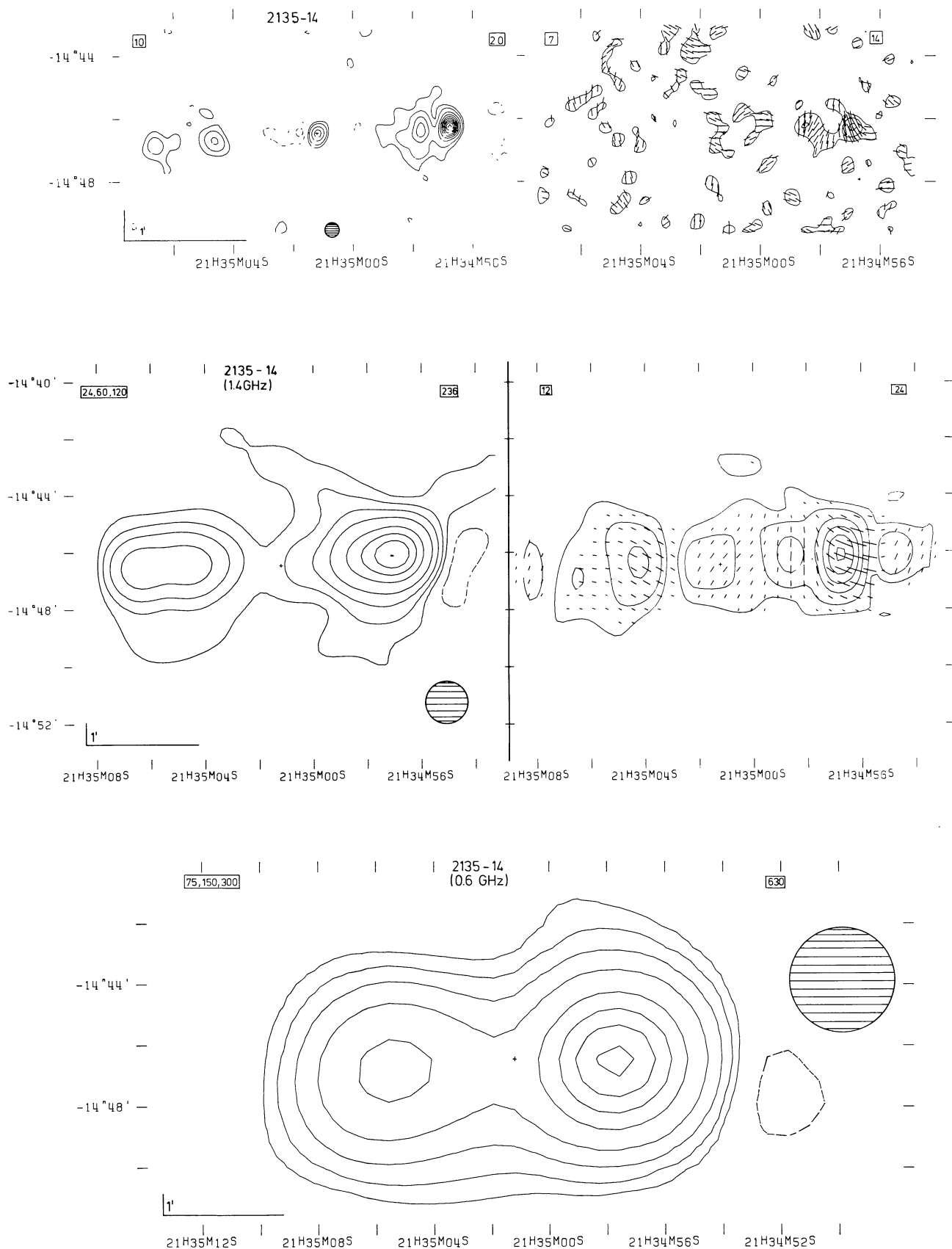


Figure 2 (continued)

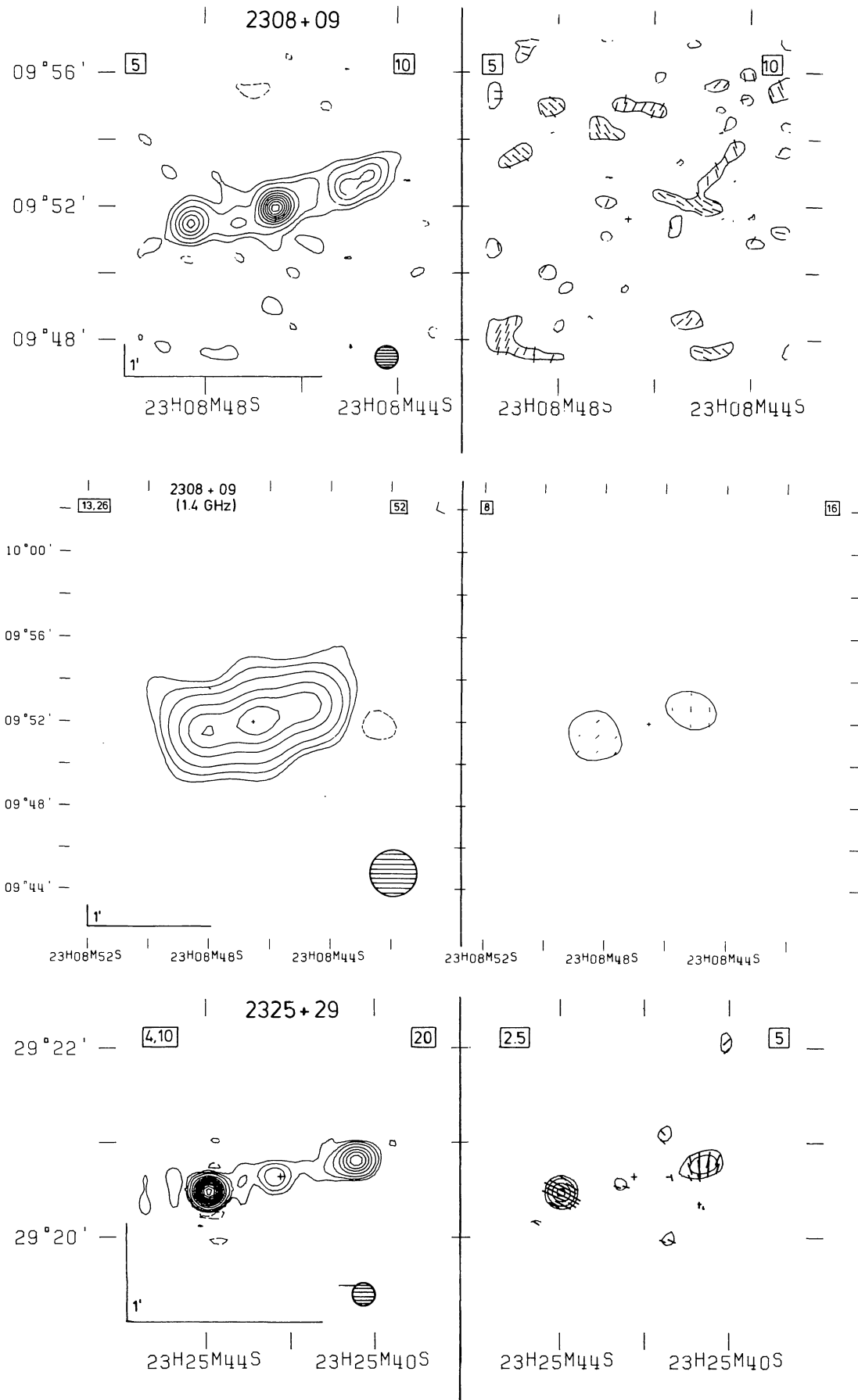


Figure 2 (continued)